

SPITZER/IRAC-MIPS SURVEY OF NGC2451A AND B: DEBRIS DISKS AT 50-80 MILLION YEARS

ZOLTAN BALOG¹

Steward Observatory, University of Arizona, 933 N. Cherry Av. Tucson, AZ, 85721

LÁSZLÓ L. KISS

Sydney Institute for Astronomy, School of Physics A28, University of Sydney, NSW 2006, Australia

JÓZSEF VINKÓ

Dept. of Optics and Quantum Electronics, University of Szeged, H-6720, Szeged, Hungary

G. H. RIEKE, JAMES MUZEROLLE, ANDRÁS GÁSPÁR, ERICK T. YOUNG
Steward Observatory, University of Arizona, 933 N. Cherry Av. Tucson, AZ, 85721

NADYA GORLOVA

Department of Astronomy, University of Florida, Gainesville, FL 32611-2055.

Draft version April 17, 2009

ABSTRACT

We present a Spitzer IRAC and MIPS survey of NGC 2451 A and B, two open clusters in the 50-80 Myr age range. We complement these data with extensive ground-based photometry and spectroscopy to identify the cluster members in the Spitzer survey field. We find only two members with 8 micron excesses. The incidence of excesses at 24 microns is much higher, 11 of 31 solar-like stars and 1 of 7 early-type (A) stars. This work nearly completes the debris disk surveys with Spitzer of clusters in the 30-130 Myr range. This range is of interest because it is when large planetesimal collisions may have still been relatively common (as indicated by the one that led to the formation of the Moon during this period of the evolution of the Solar System). We review the full set of surveys and find that there are only three possible cases out of about 250 roughly solar-mass stars where very large excesses suggest that such collisions have occurred recently.

Subject headings: (Galaxy:) open clusters and associations: individual (NGC 2451); (stars:) circumstellar matter; (stars:) planetary systems: protoplanetary disks; infrared: stars

1. INTRODUCTION

Studying the evolution of disks around young stars offers the opportunity to understand the formation of planetary systems and the process that leads to the formation of terrestrial planets. Protoplanetary disks accrete their gas content and evolve into debris disks (produced by the collision of larger sized bodies) on a timescale of 10 million years. The signatures of debris disks appear as mid-IR excess emission. The fraction of stars displaying mid-IR excess and the magnitude of the excess appears to decrease with time. On top of this overall trend, a few individual stars show extremely large excesses even at several hundred million years. Determining the nature and frequency of the events producing those excesses promises to provide an important perspective on planetary system evolution.

The 30 - 150 Myr range is especially interesting since Canup (2004) and Touboul et al. (2007) showed that the Earth-Moon system was formed by a collision about 30-150 Myr after the Solar System was formed. Gorlova et al. (2007) called attention to a ≈ 35 Myr old system with a large amount of debris that might have

resulted from such a giant collision. Rhee et al. (2008); Gorlova et al. (2004); Rieke et al. (2005) and Su et al. (2006) also identify young debris systems with large $24\mu\text{m}$ excesses.

NGC 2451A and B are two young open clusters projected on each other along the same line of sight that are within this interesting age range. Several attempts have been made to separate the two clusters and to determine the physical parameters of each one of them. Platais et al. (2001) analysed photometric and spectroscopic data and used proper motions and radial velocities to select members of NGC2451A. They fit theoretical isochrones to the cluster color-magnitude diagram (CMD) to calculate its distance, reddening, and age. They derived $d=188$ pc, $E(B-V)=0.01$ and $\text{age}=60$ Myr. Hünsch et al. (2003) carried out an X-ray study of the two clusters and identified 39 members of the A and 49 of the B cluster using combined X-ray and optical data. They derived distances of 206 pc and 370 pc, with corresponding ages of 50-80 Myr and 50 Myr for NGC2451A and B, respectively. Hünsch et al. (2004) completed the X-ray study with high-resolution spectroscopy and refined the membership of the two clusters. The most recent distance and age estimate was performed by Kharchenko et al. (2005). They estimated distances of 188 pc and 430 pc and ages of 57.5 Myr and

Electronic address: zbalog@as.arizona.edu

¹ on leave from Dept. of Optics and Quantum Electronics, University of Szeged, H-6720, Szeged, Hungary

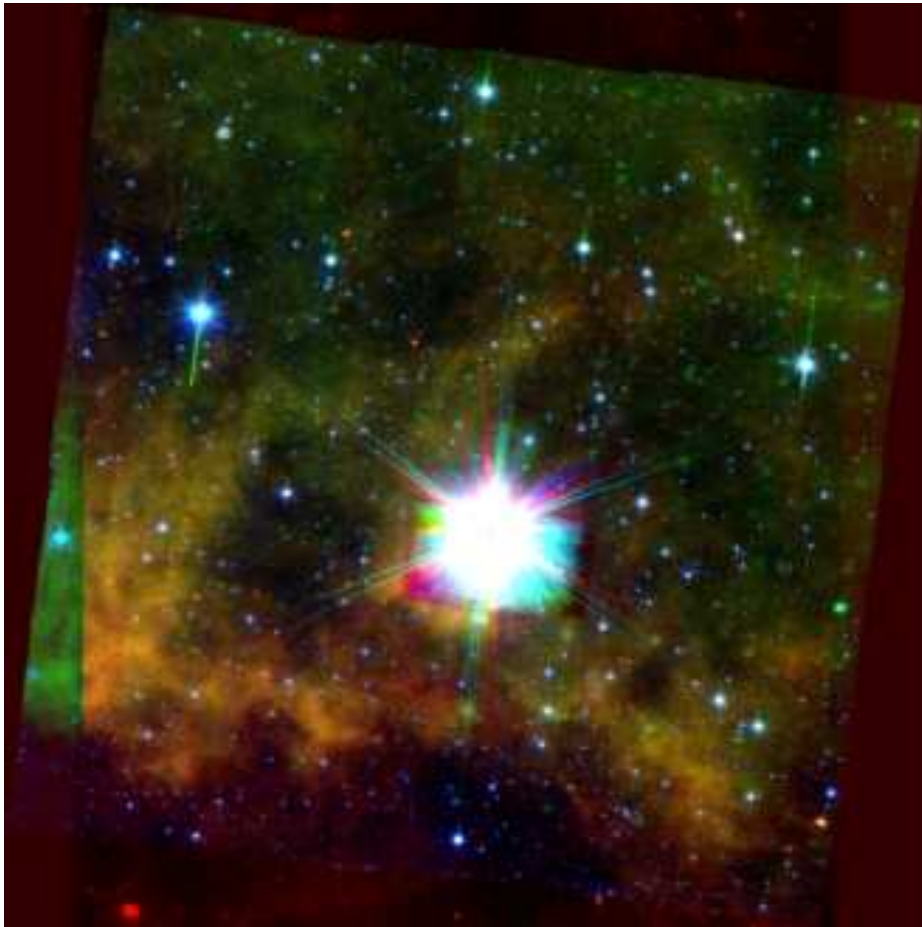


FIG. 1.— False color image of the center of NGC 2451. Blue: 4.5 μm ; Green: 8 μm ; Red: 24 μm

75.9 Myr for NGC2451 A and B, respectively. However, their analysis was based on only a handful of member candidates (26 and 11 for NGC 2451A and B, respectively) in contrast with Hünsch et al. (2003). Therefore we adopt the Hünsch et al. (2003) distances and ages and reddening ($E(B-V)$ of 0.01 and 0.05 for NGC2451 A and B, respectively) for our analysis.

In this paper we report on a *Spitzer* IRAC and MIPS survey of the central region of the clusters to study the incidence of infrared excesses in the 50-80 Myr age range. We supplement our *Spitzer* observations with a large-scale spectroscopic and optical photometric program to refine and extend our knowledge of the membership of these clusters.

2. OBSERVATIONS

2.1. *Spitzer*/IRAC and MIPS data

Observations of NGC2451 were obtained on 2004 March 02 with IRAC (Fazio et al. 2004). The IRAC survey covers about 0.6 square degree centered on HD 63032, a K2.5Ib star. The 12s high-dynamic-range mode was used to obtain two frames in each position, one with 0.4s exposure time and one with 10.4s. The observation of each field was repeated twice with a small offset, providing 20.8s integration time for each position. The frames were processed using the Spitzer Science Center (SSC) IRAC Pipeline v14.0, and mosaics were created from the basic calibrated data (BCD) frames using a custom IDL program (see Gutermuth et al. (2008) for details). Due

to the 7 arcmin offset between channel 1/3 and channel 2/4 the total area covered in all four channels is about 0.45 sq degree.

Source finding and aperture photometry on these images were carried out using PhotVis version 1.10, which is an IDL-GUI based photometry visualization tool (see Gutermuth et al. (2004) for further details on PhotVis). The radii of the source aperture, and of the inner and outer boundaries of the sky annulus were 2.4, 2.4 and 7.2 arc-second, respectively. The calibration used large aperture measurements of standard stars. The zero point magnitudes of the calibration were 19.6642, 18.9276, 16.8468, and 17.3909 corresponding to zero point fluxes of 280.9, 179.7, 115.0, 64.13 Jy for channels 1, 2, 3, and 4, respectively. Aperture corrections of 0.21, 0.23, 0.35 and 0.5 mag were applied for channels 1, 2, 3, and 4 to account for the differences between the aperture sizes used for the standard stars and for the NGC 2451 photometry.

We accepted as good detections those with photometric uncertainties less than 0.2 mag, which allowed limiting magnitudes of 18.2, 17.5, 15.4 and 14.8 at 3.6 μm , 4.5 μm , 5.8 μm , 8.0 μm , respectively. We detected almost 30000 sources at 3.6 μm , more than 20000 at 4.5 μm , and over 4000 and 3000 in the 5.8 μm and 8.0 μm images. There are more than 2500 sources that were detected in all 4 channels. Based on the 2MASS magnitudes of the detected sources, the limiting mass of our survey is $< 0.1 M_{\odot}$ for NGC2451 A and around $0.15 M_{\odot}$ for NGC2451 B.

The MIPS (Rieke et al. 2004) 24 μm survey was obtained on 2004 Apr. 11. It covers about 0.8 square degrees centered on the same position as the IRAC survey. The observations were carried out in scan map mode. The frames were processed using the MIPS Data Analysis Tool (Gordon et al. 2005). We used PhotVis to extract the sources in the 24 μm image and PSF fitting in the IRAF/DAOPHOT package was used to obtain photometry. We used a 0.59 mag aperture correction and a 7.17 Jy zero point to convert our PSF photometry to the 24 μm magnitude scale. Similarly to the IRAC photometry we also discarded sources with errors larger than 0.2 mag, leaving 2625 sources in our MIPS sample. The limiting magnitude of our 24 μm survey is 11.8, which corresponds to masses of 0.55 M_{\odot} (early M spectral type) and 0.9 M_{\odot} (early K spectral type) for stars with pure photospheric emission at the distance of NGC2451 A and B, respectively.

Fig 1 shows the false color image of the center of NGC 2451.

2.2. Optical photometry

The optical observations were made with the SITE 2048-#6 CCD camera attached to the 1.5 m telescope at CTIO on 2003 Jan. 22, 23 and 24. The camera was mounted at the f/13.5 focal position, covering a 15×15 arcmin² field-of-view with a resolution of 0.43 arcsec/pixel for the entire 2048×2048 pixel² area. The observations were made through Johnson-Cousins *UBVRI* filters, from the Tek #1² filter set.

The whole cluster was covered by $4 \times 3 = 12$ CCD frames centered on and around the brightest inner area at R.A. = 07 : 45 : 20, DEC = -38 : 02 : 00. One off-cluster area (separated by ~ 1.5 deg from the cluster center) was also imaged to sample the galactic foreground/background object population in the same line-of-sight. Each field was imaged three times through the same filter. One frame was obtained with a short exposure time (10 s for *U* and 5 s for *BVRI*) and the other two frames were taken with a longer one (250 s for *U*, 70 s for *B* and 50 s for *VRI*).

The reductions of the raw frames were performed with standard routines using *IRAF*³. After trimming the edges of the frames and subtracting the bias level from each image, the frames were divided by a master flat field image obtained by median combining the available flat field frames for each filter. Both dome flats and sky flats were taken at the beginning of each night and combined together into the master flat frames. After flat field division, the two long-exposure frames corresponding to the same filter were averaged to increase the signal-to-noise.

The photometry of the cluster frames was computed via PSF-fitting using DAOPHOT implemented in *IRAF*. A 2nd order spatially variable PSF (`varorder=2`) was built for each frame to compensate for distortions of the PSFs due to either the optical imaging artifacts in the large field-of-view, or guiding errors that occurred randomly on a few frames. For the PSF-model, `function=auto` was selected, i.e. each built-in PSF-function was computed and the best-fitting one was

adopted automatically. In most cases the `penny1` or the `penny2` function was the best-fitting one. The PSF-stars were selected interactively from a sample of the ~ 50 brightest, non-saturated stars on each frame, omitting the ones with suspicious profiles and/or detectable neighbors within $r = 15$ pixels. The `fitrad` parameter was set as 5 pixels corresponding roughly to the FWHM of the frames with the lowest quality. The detection threshold was fixed at the 4σ level on each frame.

Inspecting the results of the PSF photometry revealed that there is a small, but significant, difference between the results of the PSF and aperture photometry of the same stellar field. This difference was about the same (within ~ 0.03 mag) for the bright stars in one field, but its amount varied from field to field, ranging from a few hundredths up to ~ 0.2 mag. The aperture photometry was computed with $r_{ap} = 8$ pixels aperture radius (about $3.4''$). The local sky level was estimated as the mode of the pixel distribution within an annulus having inner and outer radii of 10 and 20 pixels, respectively, centered on each object. Because r_{ap} was more than twice the stellar FWHM for most frames, much of this difference was probably due to the distorted stellar PSFs mentioned above, plus the problems in determining the local sky level during the PSF-fitting. Therefore, we fixed the zero point of the photometry by selecting a bright, unsaturated, uncrowded reference star on each frame, and using its magnitude from aperture photometry as a reference level. Thus, the final instrumental magnitudes were determined as follows: first, differential magnitudes were computed between the PSF-magnitudes of all stars and the reference object, then the magnitude of the reference object from aperture photometry was added to each differential magnitude. For the short-exposure frames, the same procedure was applied, but for the reference object the magnitudes from the long-exposure frames were selected, thus ensuring a common zero point for the photometry of the long- and short-exposure frames.

The transformation of the CTIO instrumental magnitudes into the standard Johnson-Cousins system was performed via observations of Landolt photometric standard sequences (Landolt 1992). The L98, L101 and RU152 standard fields were imaged through each filter, weather and time permitting, on each night at different airmasses (up to 4 different elevations in the case of the L98 field). Since photometric accuracy is essential for the conclusions of this paper, we give the details of our calibration and standard transformation below.

The following formulae were adopted for converting the instrumental magnitudes into standard ones:

$$V - (v - k_v X) = \alpha_{CI} \cdot CI + \zeta_V, \quad (1)$$

$$CI = \beta_{CI} \cdot (ci - k_{ci} X) + \zeta_{CI}, \quad (2)$$

where v and ci are the instrumental V -magnitude and color index ($u - b$, $b - v$, $v - r$ or $v - i$), V and CI are the standard magnitudes and colors, X the airmass, the k s are the extinction coefficients, α_{CI} and β_{CI} are the color-dependent transformation slopes (the color terms), and the ζ s are the zero points.

Because the first night was nearly photometric, we decided to determine the color terms and the extinction coefficients from the magnitudes of standard stars observed that night. The instrumental magnitudes of these

² <http://www.ctio.noao.edu/instruments/filters>

³ *IRAF* is distributed by NOAO which is operated by the Association of Universities for Research in Astronomy (AURA) Inc. under cooperative agreement with the National Science Foundation

TABLE 1
TRANSFORMATION COEFFICIENTS DERIVED FROM LANDOLT
STANDARDS OBSERVED ON 2003 JAN.22.

Coefficient	V	$(U - B)$	$(B - V)$	$(V - R)$	$(V - I)$
k	0.15	0.15	0.13	0.00	0.05
α	—	—	0.035	—	0.031
β	—	1.064	0.880	1.055	1.021
ζ	-2.457	-1.848	-0.133	-0.083	0.822

TABLE 2
TRANSFORMATION ZERO POINTS FOR THE THREE NIGHTS

Date	ζ_V	ζ_{U-B}	ζ_{B-V}	ζ_{V-R}	ζ_{V-I}
2003 Jan 22	-2.457	-1.848	-0.133	-0.083	0.822
2003 Jan 23	-2.470	-1.770	-0.133	-0.083	0.800
2003 Jan 24	-2.486	-1.768	-0.134	-0.082	0.802

stars were computed from aperture photometry using the same aperture and annulus radii as mentioned above for the cluster frames. The transformation coefficients were then derived by fitting Eq.1 and 2 to the instrumental and standard magnitudes via χ^2 -minimization. Table 1 lists the parameters for each filter combination (note that both $(B - V)$ and $(V - I)$ were applied as the color index in Eq.1).

With the parameters listed in Table 1 determined, the color terms and extinction coefficients were kept fixed and only the zero points were fitted to the data for standard stars observed on the next two nights. Because we experienced slightly variable transparency during the second night, we have not attempted to adjust the extinction correction coefficients to achieve the best fit. The variation of the zero points (collected together in Table 2) is under 0.01 mag except for $(U - B)$, illustrating the stability of the photometric conditions at the CTIO site during our observing run.

Inserting the coefficients from Table 1 and 2 into Eq.1 and 2, the photometric data for the stars in the cluster fields have been transformed into the standard system. This resulted in a final sample of $\sim 29,000$ stars having calibrated photometry in at least the

V and I filters with uncertainties less than 0.1 magnitude.

The quality and the stability of the whole photometry

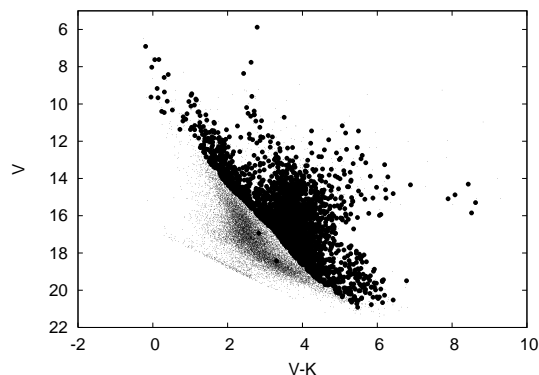


FIG. 2.— Spectroscopic sample on the V vs $V-K$ diagram. Large dots: targets with spectra, small dots: all stars with available V and K magnitudes in the whole cluster area

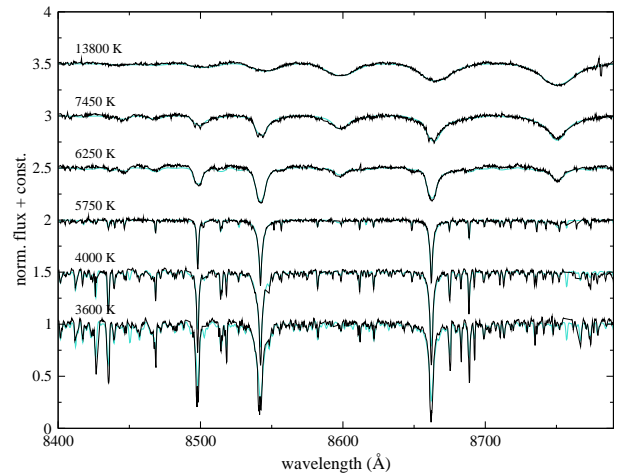


FIG. 3.— Observed stellar spectra (light blue/gray lines) and the best-fit synthetic data from the Munari et al. (2005) spectrum library (black lines).

including the standard transformation has been verified by comparing our standard V and $B-V$ magnitudes with those from Platais et al. (2001) for the ~ 1800 stars in common between the two samples. The agreement is very good. The mean difference between the two samples is 0.001 ± 0.06 mag in V and -0.007 ± 0.04 mag in $B - V$ (the errors are the RMS of the residuals), thus, statistically insignificant. Therefore our new CCD photometry in the field of NGC 2451 results in a sample containing $\sim 29,000$ stars with calibrated data. This nearly doubles the amount of photometric data available for this field.

2.3. Radial velocity survey

We acquired AAOmega data using the Anglo-Australian Telescope at Siding Spring, Australia on three nights, February 15, 16 and 17, 2008, in acceptable conditions (clear skies with 1.5-2.5 arcsec seeing). In the blue arm we used the 2500V grating, providing $\lambda/\Delta\lambda = 8000$ spectra between 4800 Å and 5150 Å. In the red arm we used the 1700D grating that has been optimized for recording the Ca II infrared triplet region. The red spectra range from 8350 Å to 8790 Å, with $\lambda/\Delta\lambda = 10000$. This setup has the highest spectral resolution available with AAOmega, suitable to measure stellar radial velocities. In total, we acquired eleven field configurations centered on the open clusters. We selected the targets for our spectroscopic campaign based on their positions in the optical-near-IR color-magnitude diagram: we targeted each source that is brighter than the 80 Myr isochrone plus 0.2 mag placed at the distance of the more distant cluster in the V vs. $V-K$ diagram. We show the spectroscopic candidates in Fig. 2 together with all the stars with available V and K photometry in the field. Our spectroscopic coverage is not complete for two reasons: (i) we concentrated our efforts to the central part of the cluster where we had *Spitzer* data; (ii) there were faint objects for which the low S/N of the spectra prevented measuring meaningful radial velocities.

The spectra were reduced using the standard 2dF data reduction pipeline. We performed continuum normalization for the stellar spectra using the IRAF task onedspec.continuum and then cleaned the strongest skyline residuals using linear interpolation of the surrounding

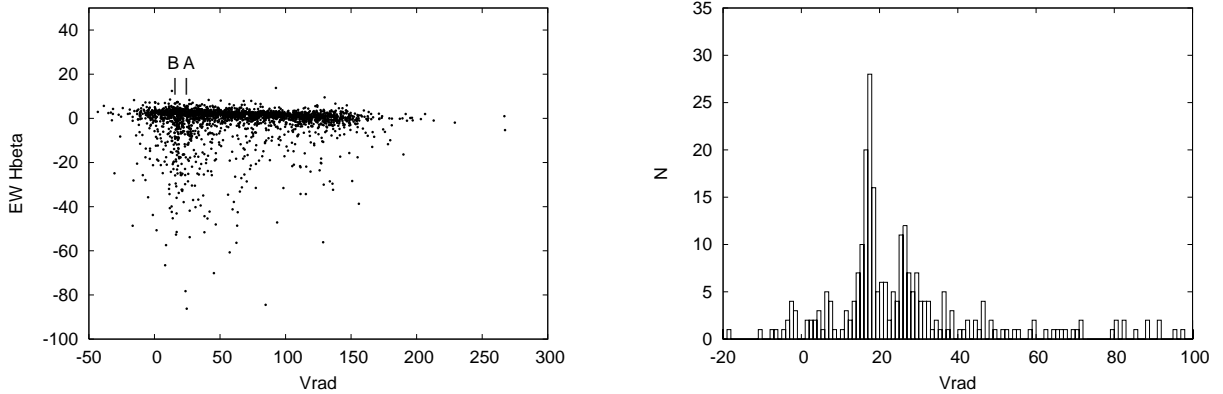


FIG. 4.— Left panel: EW of $H\beta$ vs radial velocity. A and B show the clusters’ mean radial velocities from Hünsch et al. (2004). Left panel: all stars, right panel: radial velocity histogram of the two clusters using stars that show evidence of chromospheric activity

continuum.

Atmospheric parameters and radial velocity were determined for each star in an iterative process, which combined finding best-fit synthetic spectrum from the Munari et al. (2005) spectrum library, with χ^2 fitting, and cross-correlating the best-fit model with the observed spectrum to calculate the radial velocity. This approach is very similar to that adopted by the Radial Velocity Experiment (RAVE) project (Steinmetz et al. 2006; Zwitter et al. 2008), and our analysis is based on the same synthetic library as RAVE. Earlier results for other star clusters with the same instrument and analysis can be found in Kiss et al. (2007, 2008). Because of the wide range of temperatures (and hence spectral features), we needed three subsequent iterations to converge to a stable set of temperatures, surface gravities, metallicities and radial velocities. The latter are believed to be accurate within $\pm 1\text{-}2 \text{ km s}^{-1}$ for the cooler stars and $\pm 5 \text{ km s}^{-1}$ for the hotter stars in the sample (the boundary is roughly at 8000-9000 K). These values have been estimated from Gaussian fits of the cross-correlation profile using the IRAF task `rv.fxcor` and should only be considered as representative numbers. The atmospheric parameters (T_{eff} , $[M/H]$, $\log g$), due to their degeneracy, are accurate to about $\pm 300 \text{ K}$ and $\pm 0.5 \text{ dex}$, with strong correlations (see Zwitter et al. (2008) for a thorough discussion of the RAVE error analysis).

To illustrate the difficulties one faces when analysing cool and hot stars together in the Ca II triplet region, we show sample spectral fits in Fig. 3. Since the Ca II lines almost exactly coincide with hydrogen lines in the Paschen series, we found that it was absolutely crucial to have the best-match template for cross-correlation. A slight template mismatch can easily lead to radial velocity shifts of several km s^{-1} at this intermediate spectral resolution and hence one has to be very careful to optimize template selection (contrary to the commonly used practice in the optical range that the same template is used across a range of spectral subtypes or even types). It is also unavoidable that as soon as the temperature reaches about 9000 K, the broad spectral features will lead to a degraded velocity precision simply because of the broadened cross-correlation profile. NGC 2451A and B, as reasonably young open clusters, still host a significant number of hotter main sequence stars, possibly resulting in degraded velocity precision for a fraction of stars.

Another difficulty was the very high incidence of Ca II emission (defined by the excess flux of the calcium lines relative to the best-fit model spectra), especially in late-type main sequence stars in the clusters. Both clusters are young, hence the high rotation rates can lead to elevated chromospheric activity, for which the Ca II lines are good indicators (Andretta et al. 2005). When comparing the best-fit models to the observed spectra, we noticed distorted Ca II profiles for many stars, frequently in the form of central emission components within the lines. These can introduce random velocity errors of up to $10\text{-}20 \text{ km s}^{-1}$ in the maximum of the cross-correlation profile. This was particularly apparent after modifying the velocity determination for 405 stars with Ca II line profile irregularities: after excluding the Ca II lines from cross-correlations, a large fraction of the refined velocities were very close to the cluster’s mean velocities (Fig.4).

We also measured cross-correlation velocities from the lower resolution blue spectra. These data were less useful because many of the stars have a broad $H\beta$ line and only a few additional weak features in the recorded wavelength range, leading to a broad cross-correlation profile and radial velocities accurate to only about $\pm 10 \text{ km s}^{-1}$.

3. ANALYSIS

3.1. Radial velocities of the clusters

The clusters are in the plane of the Milky Way so the background contamination overwhelms the cluster members. To estimate the radial velocities of the clusters we need to make some assumptions to separate the probable cluster members from the field based on our present knowledge of the cluster. Based on the young age of the clusters, we assumed that our sample should contain a large number of K and M dwarfs that show chromospheric activity, i.e., signs of emission in the CaT lines. We identified 405 active red objects in our sample. Several of our target stars show sharp $H\beta$ emission as additional evidence for activity. In the left panel of Fig. 4 we show the equivalent width of $H\beta$ vs radial velocity (negative EWs mean emission). We see two distinct groups of emission line objects in the figures around the approximate position of the radial velocity values of NGC2451 A and B (22.7 km s^{-1} and 14 km s^{-1}) that were estimated by Hünsch et al. (2004). We show the radial velocity histogram of these stars in the right panel of Fig. 4. From this histogram we calculate mean radial velocities $26.7 \pm 2.4 \text{ km s}^{-1}$ and $17.4 \pm 2 \text{ km s}^{-1}$ for NGC2451 A and

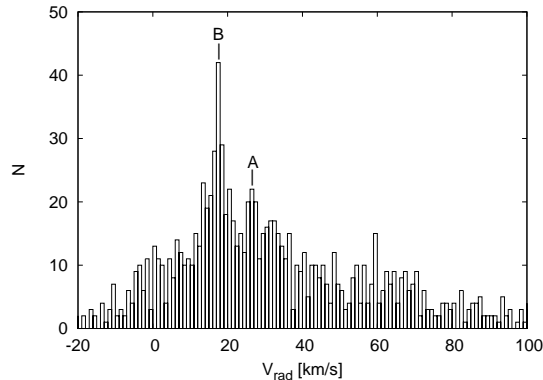


FIG. 5.— Radial velocity histogram of the two clusters using all stars with $\log g > 3.0$. A and B show the radial velocity values determined using the chromospherically active young stars for NGC 2451 A and B, respectively.

B, respectively. Because chromospheric activity is not always present in young stars (e.g. early type ones) we use this test only to estimate true cluster velocities.

Our average radial velocity values are about 3 km s^{-1} higher than those of Hünsch et al. (2004). Considering the formal standard deviation of the Hünsch et al. (2004) data (2.3 km s^{-1} for cluster A and 2.5 km s^{-1} for cluster B) and the small number of member stars in that sample (21 for cluster A and 10 for cluster B), the 3 km s^{-1} systematic difference is hardly significant. Given that our sample contains three-to-ten times more members for each cluster, we adopt our mean values for the cluster velocities.

3.2. Cluster membership and color magnitude diagrams

In Fig. 5 we show the radial velocity histogram of our complete sample with $\log g > 3$ (giants filtered out). The two peaks at the positions of the radial velocities of the two clusters (designated with A and B) are readily distinguishable. However a large number of contaminating stars might be present due to the strong galactic background so the radial velocity is not enough to determine accurate membership status. Therefore, we used photometric diagrams also to clean our initial sample.

We performed the final determination of memberships as follows. We selected member candidates using the radial velocity and $\log g$ criteria. We accepted all objects as cluster members that had $\log g > 3$ (1079 out of 2570 objects satisfied this criterion) and not more than a 2σ deviation from the clusters' mean radial velocities ($13.4 \text{ km s}^{-1} < V_{\text{rad}} < 21.4 \text{ km s}^{-1}$ for NGC2451 B and $21.9 \text{ km s}^{-1} < V_{\text{rad}} < 31.5 \text{ km s}^{-1}$ for NGC2451 A, 152 and 200 objects for NGC2451 A and B, respectively). Then we plotted the initial sample in color magnitude diagrams and removed the objects with positions inconsistent with the 50 Myr isochrone of Siess et al. (2000) at the distance of the clusters. We show the final cleaned diagrams in Fig 6. Our final sample consists of 60 objects in NGC2451 A and 121 objects in NGC2451 B. The photometry of the members is listed in Tables 3, 4, 5, and 6.

3.2.1. Members from Platais et al. (2001)

There are 18 members of NGC2451 A reported by Platais et al. (2001) in the area covered by all 5 bands of our *Spitzer* observations. Thirteen of them were included in our radial velocity survey. We rejected 7 of these stars

based on their radial velocity; 4 were included in our clean NGC2451 A membership list while 2 have radial velocities just outside the 2σ limit. We included these two stars along with the other 5 not covered by the radial velocity survey in our final sample for NGC2451 A (they are marked with filled squares in the plots in the left column of Fig 6). We used the Platais et al. (2001) magnitudes for these objects because they were not detected by our UBVR survey. As a result, they are not plotted in the V vs V-I plot in Fig 6

3.2.2. Members from Hünsch et al. (2003) and Hünsch et al. (2004)

Hünsch et al. (2003) list 87 objects in the field of our *Spitzer* survey as candidate members of either NGC2451 A or B. Unfortunately the coordinates given in Hünsch et al. (2003) are from X-ray data and have sufficiently large uncertainties that it is not easy to identify their sources in the IRAC and MIPS datasets. We could identify 58 sources out of 87 with a detection in at least one *Spitzer* band. Thirty four of them were included in our radial velocity survey which also included 7 stars identified as non-members by Hünsch et al. (2003).

In the case of NGC 2451 A, sixteen Hünsch et al. (2003) members are included in our radial velocity survey, which confirms the membership status of 10. In NGC2451 B we have 13 Hünsch et al. (2003) members in our spectroscopic sample. Eight of them are confirmed as members by the radial velocity data while two have radial velocities indicating that they are members of NGC2451 A. We can reject 3 Hünsch et al. (2003) members based on their radial velocity data. There is a third group of Hünsch et al. (2003) stars that contains objects that might be members of either of the clusters. Six of them are included in our radial velocity survey. Based on the radial velocity data we confirm membership of 5 objects (4 in NGC2451 A and 1 in NGC2451 B). We included the Hünsch et al. (2003) members without radial velocities in our final sample if they were detected in at least one of the *Spitzer* bands (3 and 10 for NGC2451 A and B, respectively). They are marked with filled triangles in Fig 6. These additions make the total number of cluster members 69 and 131 for NGC2451 A and B, respectively. We detect 22 members at $24 \mu\text{m}$, 47 at 8 and $4.5 \mu\text{m}$, and 49 at 5.8 and $3.6 \mu\text{m}$ in NGC2451 A. In NGC2451 B we detect 20 members at $24 \mu\text{m}$, 92 at $8 \mu\text{m}$, 96 at $5.8 \mu\text{m}$, 94 at $4.5 \mu\text{m}$, and 98 at $3.6 \mu\text{m}$. Our detection rate in the IRAC bands is about 70% in both clusters while at $24 \mu\text{m}$ it is 32% in NGC2451 A and 15% in NGC2451 B, respectively. These detection rates are very similar to that of Gorlova et al. (2007) for the ~ 35 Myr old cluster NGC2457. In the following we use only the sources that are detected in all four IRAC bands or detected at $24 \mu\text{m}$.

4. IDENTIFYING EXCESS CANDIDATES

4.1. IRAC excesses

The four IRAC bands covering the $3.6\text{--}8 \mu\text{m}$ regime of the spectrum trace dust from the near-sublimation temperature of 1000 to 400 K, corresponding to radii within 1 AU for solar-type stars. We can identify $8 \mu\text{m}$ excesses from the IRAC data, if we plot K-[8] vs V-K. Fig 7 shows the V-K vs K-[8] color-color diagram of NGC2451 A (left panel) and B (right panel). The large baseline of the V-K color makes this filter combination an ideal choice for

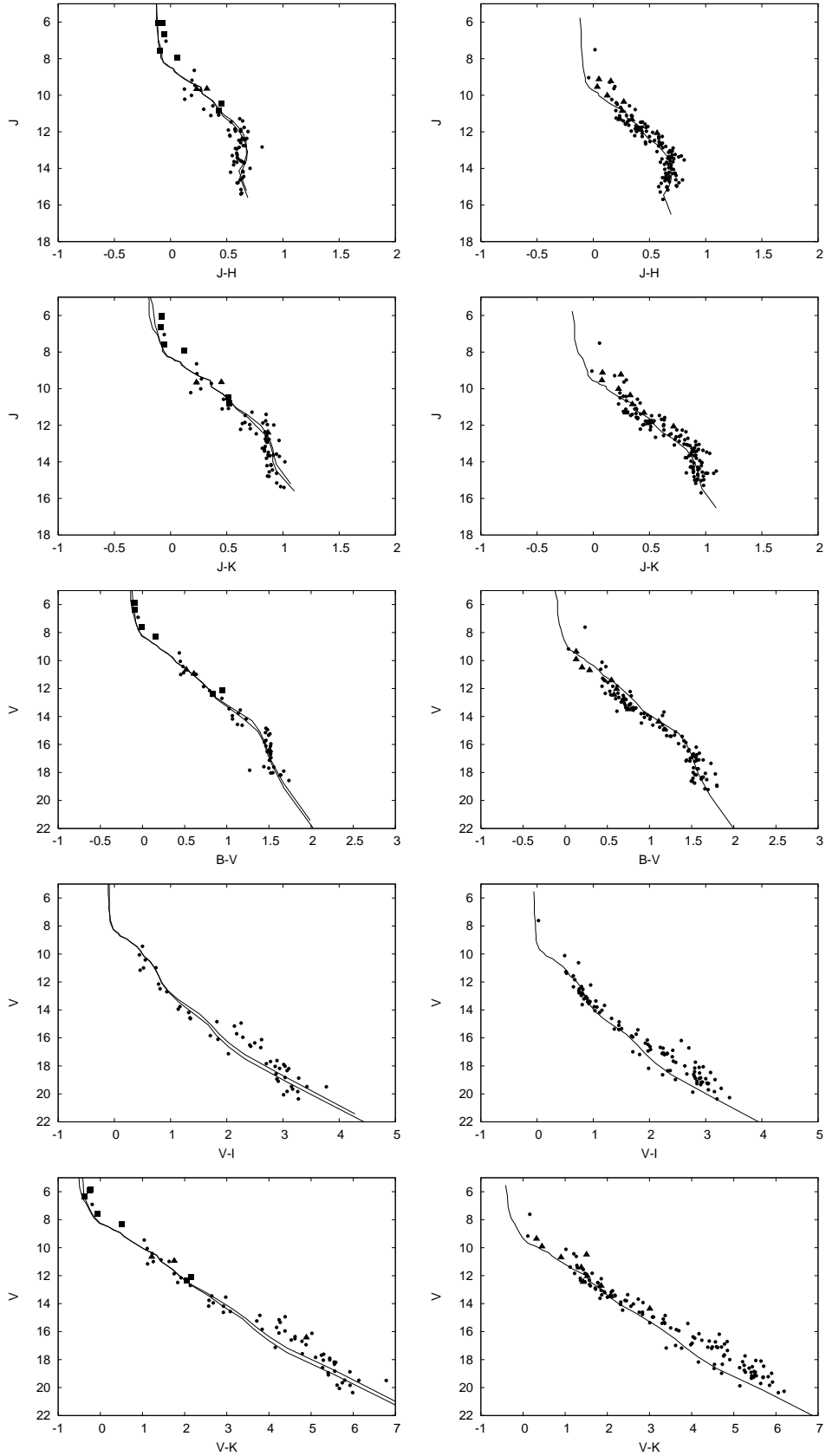


FIG. 6.— Color-magnitude diagram of the members of the two clusters (left panel: NGC2451 A; right panel: NGC2451 B). dots: stars in our spectroscopic survey, squares: members from Platais et al. (2001) not included in our spectroscopic sample, triangles: members from Hünsch et al. (2003) not included in our spectroscopic sample. The solid line show the 50Myr and 80Myr isochrone of Siess et al. (2000) for NGC2451 A and the 50 Myr isochrone of Siess et al. (2000) for NGC2451 B, shifted with the distance and extinction of Hünsch et al. (2003)

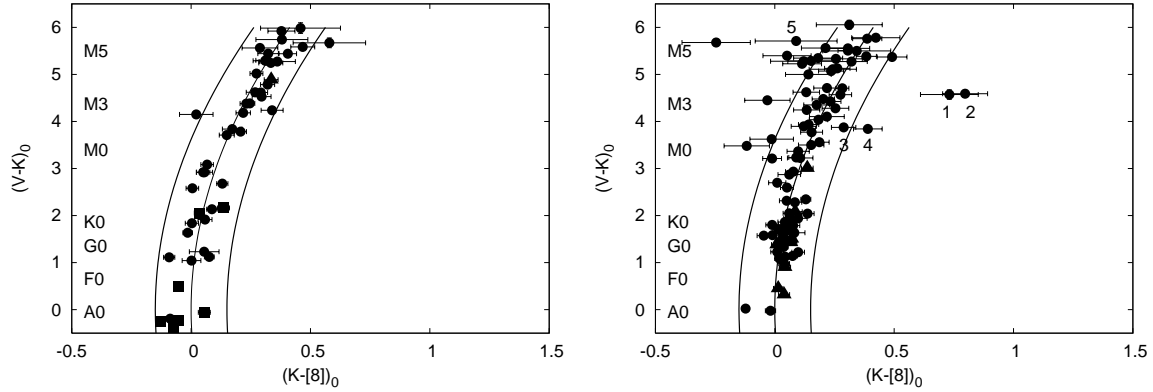


FIG. 7.— V-K vs K-[8] diagrams of NGC 2451 A (left panel) and B (right panel). The meaning of the symbols is the same as in Fig 6. Horizontal error bars show the 1σ photometric errors. The solid lines represent the color-color relation for normal stars and its 3σ limits.

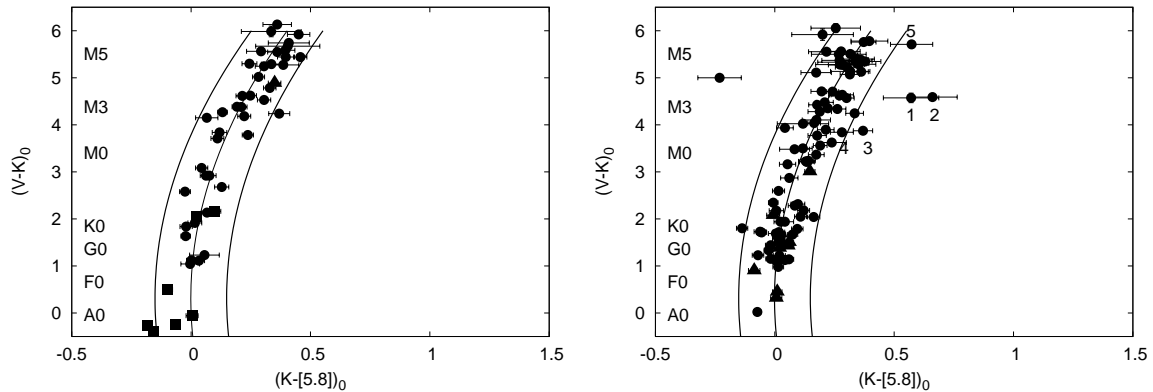


FIG. 8.— The same as Fig 7 but for V-K vs K-[5.8].

photometric spectral type determination given the low reddening of the clusters. There is a monotonic relationship between increasing V-K and stellar spectral type that results in a narrow locus, extending from early to late type stars; the scatter in this locus increases for $V-K > 5$ due to measurement errors. Objects to the right of this locus are stars with excesses at $8\mu\text{m}$.

The robust determination of cluster membership allows us to establish a good color-color relation for 50-80 Myr clusters by fitting a 2nd degree polynomial to the locus of the V-K - K-[8] and V-K - K-[5.8] diagrams. We merged the data of the two clusters to increase the number of sources in the fit and required both colors of an A0 star to be 0. Eq. 3 and 4 show the results of the fit which is also shown with a solid line on Fig 7 and 8. The rms of the datapoints around the fit is 0.05 in both colors.

$$(K_S - [8])_0 = 0.0115 \pm 0.0011(V - K_S)_0^2 - 5.89 \times 10^{-5} \pm 0.0053(V - K_S)_0 \quad (3)$$

$$(K_S - [5.8])_0 = 0.0125 \pm 0.0012(V - K_S)_0^2 - 0.0078 \pm 0.0060(V - K_S)_0 \quad (4)$$

No star with $8\mu\text{m}$ excess (relative to K) was detected in NGC2451 A and only two candidate excess stars (#1 and #2) and another two weak possible excess candidates (#3 and #4) were detected in NGC 2451 B. We also plot the same diagrams but using the IRAC $5.8\mu\text{m}$ channel

on Fig 8. This diagram allows us to check whether our $8\mu\text{m}$ detections are real or are just a result of some anomaly in the image (e.g. a cosmic ray hit). Both $8\mu\text{m}$ excess candidates are confirmed by having excess at $5.8\mu\text{m}$ also. However star #2 has a close companion that might compromise the $8\mu\text{m}$ and $5.8\mu\text{m}$ photometry (see Fig 10). Stars #3 and #4 are also situated slightly to the right of the main locus of sources in V-K vs K-[5.8], however, #3 has a larger excess at $5.8\mu\text{m}$ so its status as an excess candidate is questionable. None of the four $8\mu\text{m}$ excess candidates were detected at $24\mu\text{m}$.

We fitted a Kurucz model to the short wavelength portion of the sources' SEDs. Fig. 11 shows the results of the fit. Based on their SEDs we can conclude that only one of the four candidates (#1) is a true excess source. The SED of #2 shows that the photometry of this source is contaminated by the nearby bright star because the excess extends over all IRAC bands. The SED of #3 shows no excess at all and that of #4 has a marginal one. The significance of the excess for #4 calculated from the photometric errors and the rms of the fit is slightly lower than 3σ .

We noticed that there is a small hint of an $8\mu\text{m}$ excess on the SED of the $24\mu\text{m}$ excess star #12 (see next section) and all but one of the A (or earlier) type stars have K-[8] colors less than zero although they are inside the 3σ limit of the trendline in Fig 7. To check the origin of this slight discrepancy we replaced K with [3.6] and used

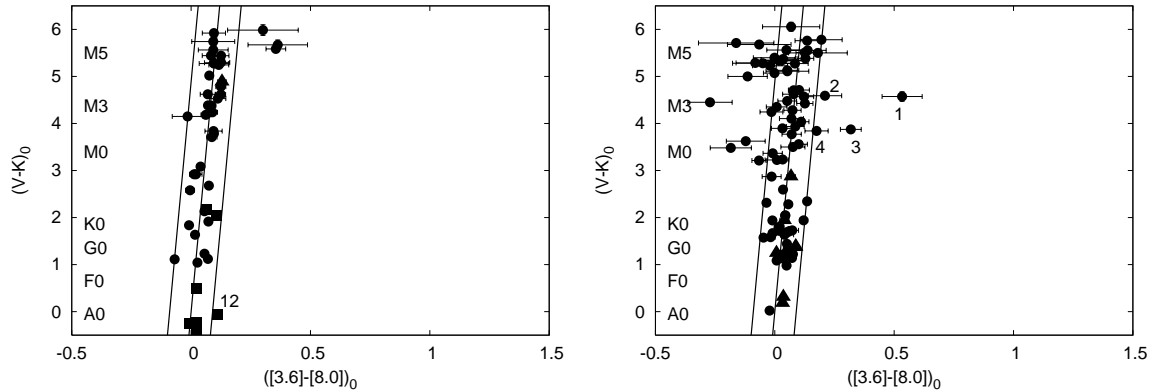


FIG. 9.— The same as Fig 7 but for V-K vs $[3.6]-[8.0]$.

the V-K vs $[3.6]-[8.0]$ diagram to detect excesses (Fig. 9). A linear relation between the V-K and the $[3.6]-[8.0]$ colors can be found for the photospheric sources

$$([3.6] - [8])_0 = 0.01842 \pm 0.001277(V - K_S)_0 \quad (5)$$

with rms scatter of 3%. We also show this relation along with the 3σ limits in Fig. 9.

In this diagram there is no systematic deviation from the main relation and it seems that #12 has a marginal excess at $8 \mu\text{m}$ relative to $3.6 \mu\text{m}$. The significance of the excess is about 4σ . There are some excess candidates among the late M type stars of NGC2451 A but their significance is less than 3σ . In the case of NGC2451 B (Fig. 9 right panel) the diagram clearly shows that the only viable $8 \mu\text{m}$ excess candidate is #1. Although #3 shows some $[3.6]-[8.0]$ excess, the SED of the source does not support it.

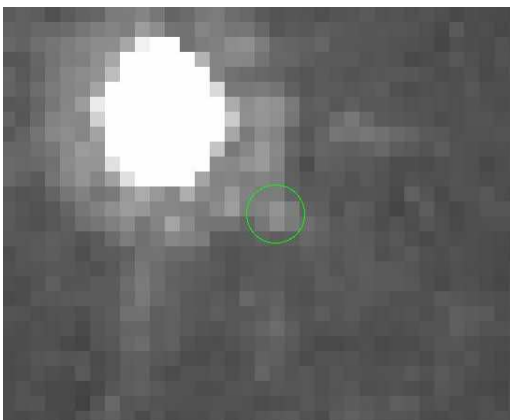


FIG. 10.— Location of star #2. The green circle shows the aperture size that was used for the photometry

To summarize, at $8 \mu\text{m}$ we have less than 2% excess fraction in NGC2451 A (one marginal excess) and a less than 1% excess fraction in NGC2451 B (one clean excess). This result is very similar to that of Gorlova et al. (2007) suggesting that IR excess shortward of $24 \mu\text{m}$ is very rare in clusters older than 20-30 Myr and indicates that the disk within 10 AU is cleared of dust for nearly all stellar systems older than 30 Myr.

4.2. MIPS excesses

Fig 12 shows the dereddened V-K vs $K-[24]$ for NGC2451 A (left panel) and NGC2451 B (right panel). Because there are too few detections to determine a zero excess locus purely from these data, for this purpose we have used a database of more than 1500 stars derived from nearly all of the Spitzer debris disk programs. The sample has good coverage from $-0.4 < V-K < 3.5$, with still a number of members up to $V-K = 8$. A simple polynomial fit has been made to the photospheric color-color locus. The rms scatter around this fit (clipping the positive outliers that have excesses) is only 3%. The locus itself is therefore very well determined and we can take a typical uncertainty for the measurement of any given star to be 3% relative to this locus (plus any statistical errors). This locus with $3-\sigma$ errors (9%) is plotted in Fig 12.

It is obvious that excess at $24 \mu\text{m}$ is far more common than at shorter wavelengths. We find 9 stars in the case of NGC2451A and 10 stars in the case of NGC2451 B to the right of the photospheric locus. However, only 7 of them in both diagrams (the numbered sources in Fig 12) are more than 3σ distance from the locus (the distance of the negative outlier left of the locus). The measured $(K-[24])_0$ color along with the predicted photospheric $K-[24]$ color of these objects and the significance of the excesses are presented in Table 7. For the prediction of the photospheric colors we used the photospheric locus shown in Fig 12. The significance was calculated using the photometric errors and the rms around this locus. To check the validity of our excess candidates (as in the previous section) we fit Kurucz model atmospheres to the short wavelength part of their SEDs. The fits are shown in Fig 13 and 14. In all cases the $24 \mu\text{m}$ flux is above the photosphere by more than 3σ , confirming the excess. The fraction of stars with excess at $24 \mu\text{m}$ is about $33 \pm 10\%$ (7/22) for NGC2451 A and $36 \pm 10\%$ (7/20) for NGC2451 B. We calculated the disk fractions and errors using Bayesian statistics as described in Gáspár et al. (2009). All but one of our $24 \mu\text{m}$ excess candidates have spectral type F or later (based on their V-K colors and fitted SEDs). We detect only one star earlier than F0 with $24 \mu\text{m}$ excess in NGC2451 A and none in NGC2451 B.

Our excess fractions among solar type stars are $35 \pm 12\%$ (5/15) in NGC251 A and $39 \pm 12\%$ (6/16) for NGC

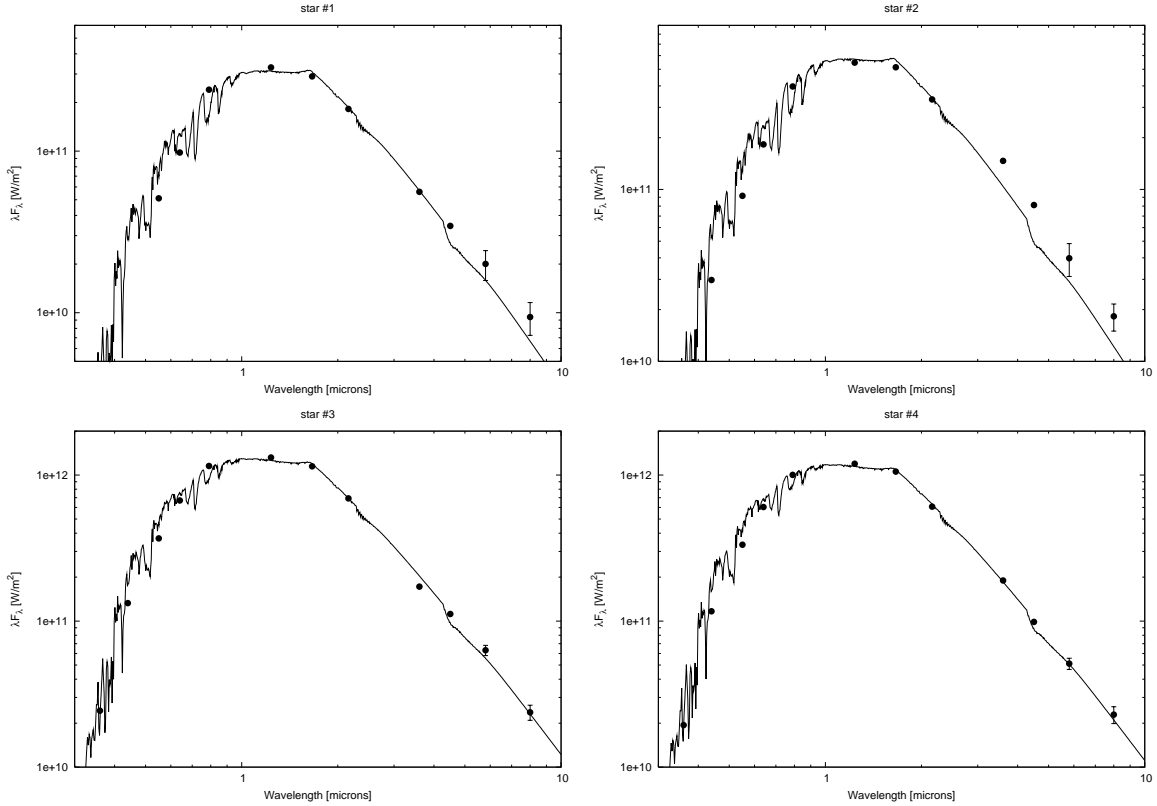


FIG. 11.— The SEDs of the $8\mu\text{m}$ excess candidates together with the fitted Kurucz atmospheric models. Errorbars at 5.8 and $8.0 \mu\text{m}$ show the 3σ photometric error.

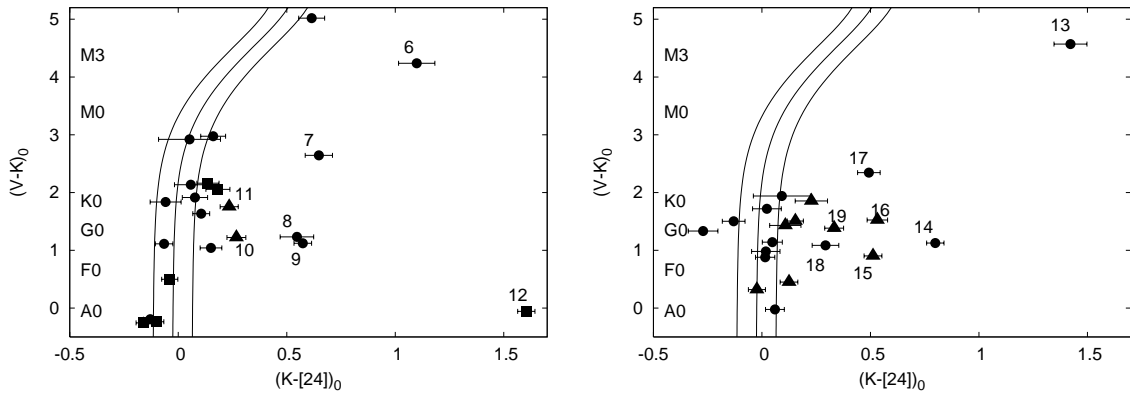


FIG. 12.— The same as Fig 7 but for V-K vs K-[24]. The solid lines represent the trendline (see text) and its 3σ limits

2451 B, and for early type stars are $29\pm 17\%$ (1/5) and $20\pm 20\%$ (0/3) for NGC2451 A and B, respectively.

5. DISCUSSION

5.1. Excess fractions

Our results for excess fraction in the solar type stars of NGC2451 B are roughly consistent with other clusters with similar ages such as IC 2391 (50 Myr - 31% (Siegler et al. 2007)) or NGC 2547 (35 Myr - 40%; (Gorlova et al. 2007)). In the case of NGC2451 A our excess fraction is significantly larger than that of M47 (80 Myr - 6% (Gorlova et al. 2004)) which might indicate that the age of NGC2451 A is closer to 50 Myr rather than 80 Myr. However, the study of M47 has a

higher threshold for detection of excesses, which might also account for the lower fraction.

For the early type stars our results are in agreement with those of Siegler et al. (2007) and Su et al. (2006) who found a very low excess fraction (about 10% and 14% for IC2391 (50 Myr) and IC2602 (30 Myr), respectively).

Fig 15 shows the disk fractions as a function of age (similar to Fig 9. of Gáspár et al. (2009)) (left panel: early type stars; right panel: late type stars). Open circles show the data from Table 4 and 6 of Gáspár et al. (2009) while filled squares designate the two new data-points from our study. We note that for stars younger than 10 Myr the excess not necessarily indicates the pres-

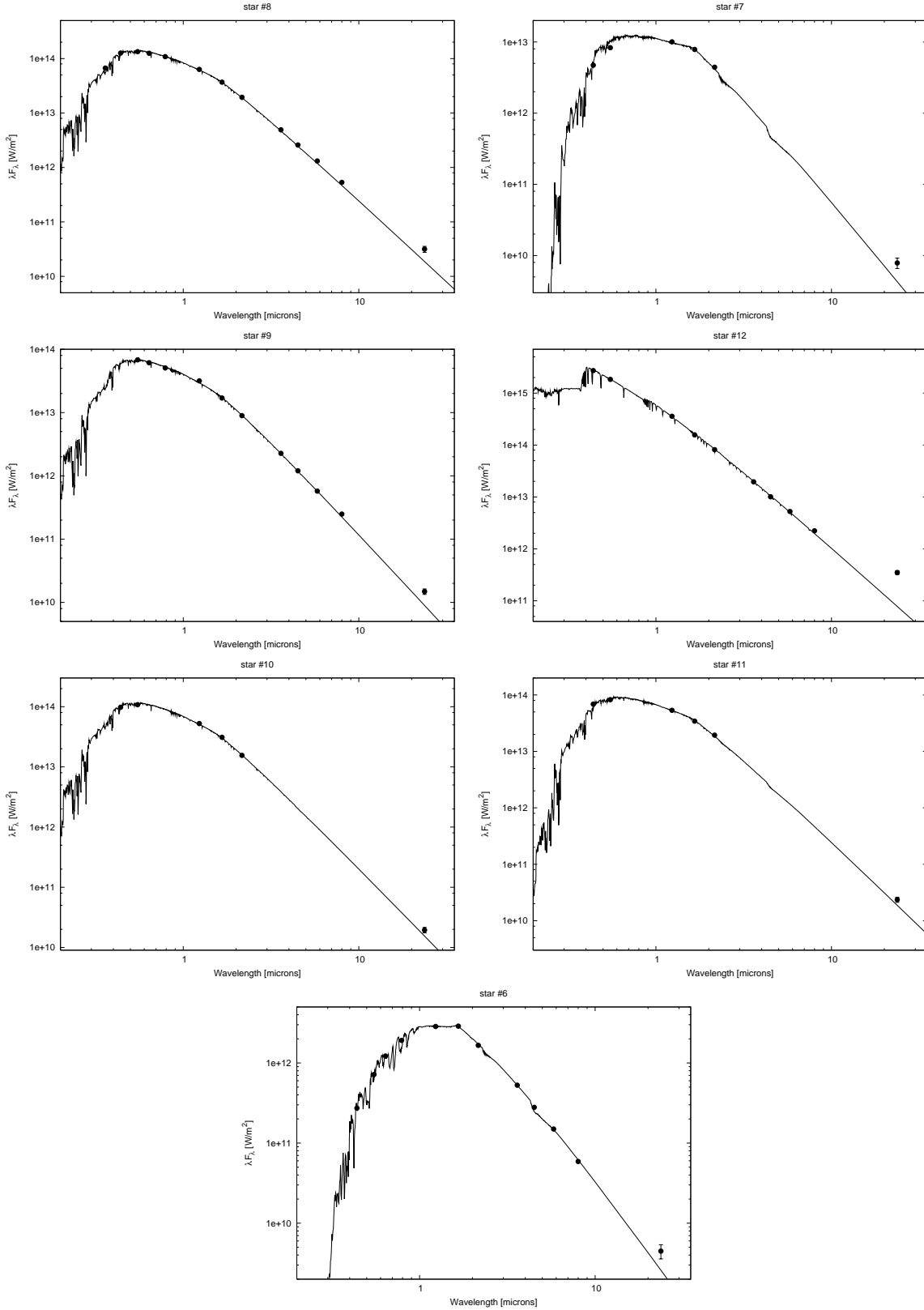


FIG. 13.— The SEDs of the $24\mu\text{m}$ excess candidates in NGC2451 A together with the fitted Kurucz atmospheric model. The errorbars represent the 3σ photometric error.

ence of debris but primordial dust left over from the star formation process as pointed out by Rhee et al. (2007), so the first three points in the figure might overestimate

the debris disk fraction. An interesting feature of the figures is that there is a dip in the fraction of debris disks in the age range of 30-80 Myr. Outside this range the decay

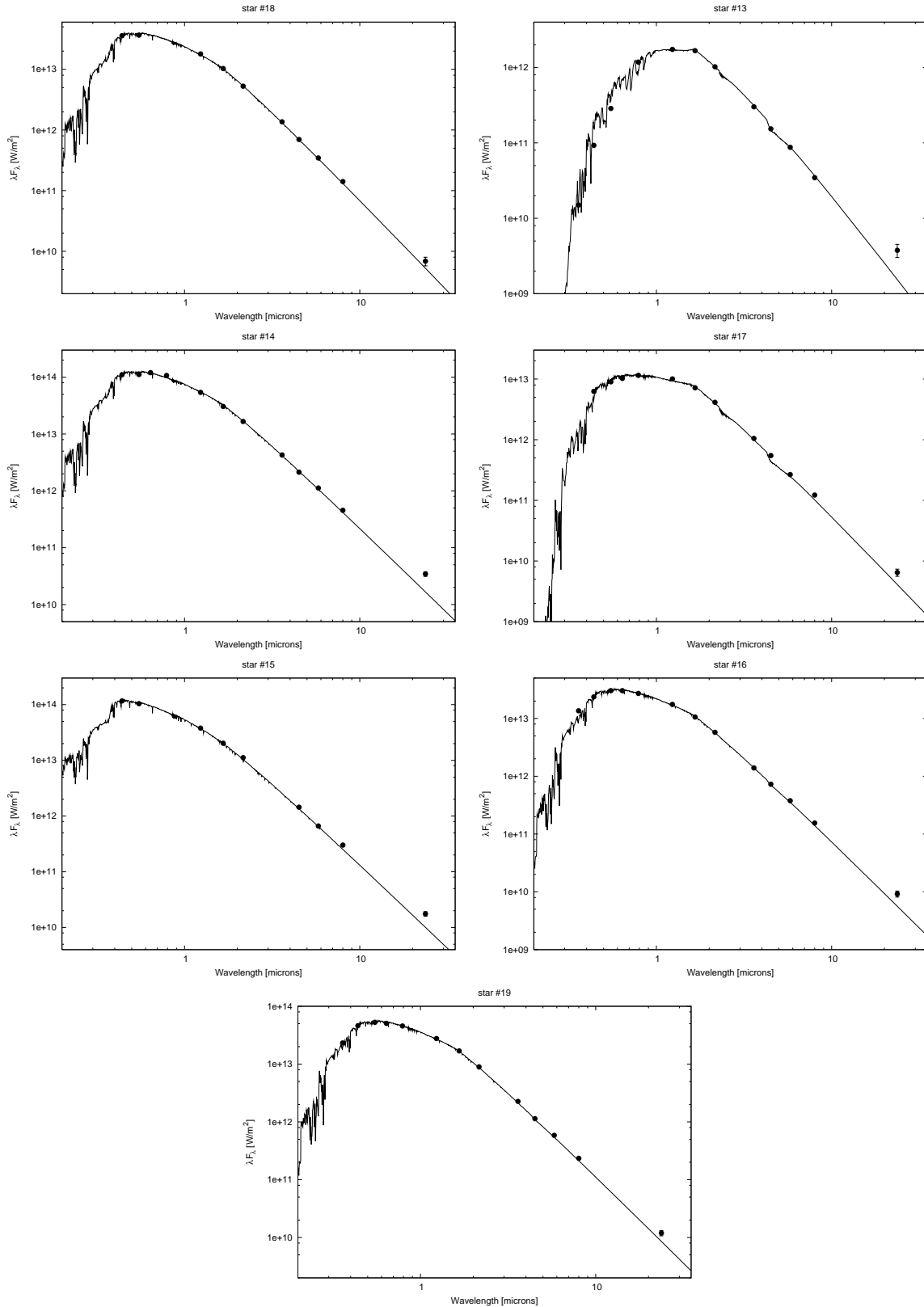


FIG. 14.— The SEDs of the $24\mu\text{m}$ excess candidates in NGC2451 B together with the fitted Kurucz atmospheric model. The errorbars represent the 3σ photometric error.

seems to be monotonic. Our two clusters slightly deviate from the main trend in the late type stars also but in a different direction. They are both situated above the

main locus of stars along with some other clusters of similar age. Incompleteness might account for the discrepancy. However, even if we remove the faintest stars (#17

TABLE 7
MEASURED AND PREDICTED PHOTOSPHERIC $(K-[24])_0$ COLORS OF CLUSTER MEMBERS
WITH $24\ \mu\text{M}$ EXCESSES

ID	RA J2000	DEC J2000	$(K-[24])_0$ mag	$\sigma((K-[24])_0)$ mag	$(K-[24])_0^{phot}$ mag	significance of excess
NGC2451 A						
#6	116.04942	-37.73994	1.099	0.084	0.271	9σ
#7	116.74747	-38.37820	0.648	0.063	0.023	9σ
#8	116.31223	-38.19624	0.547	0.077	-0.018	7σ
#9	116.23017	-38.07956	0.574	0.041	-0.019	12σ
#10	116.53718	-37.39910	0.268	0.043	-0.018	5σ
#11	116.10025	-38.59977	0.235	0.042	-0.011	5σ
#12	116.18701	-38.05376	1.604	0.040	-0.024	33σ
NGC2451 B						
#13	116.67488	-37.98390	1.422	0.076	0.353	13σ
#14	115.95562	-37.89574	0.799	0.040	-0.022	17σ
#15	116.21267	-37.66869	0.496	0.041	-0.023	11σ
#16	116.50776	-38.00752	0.516	0.047	-0.022	10σ
#17	116.44107	-37.89720	0.493	0.052	-0.010	9σ
#18	116.74249	-37.63916	0.293	0.061	-0.024	5σ
#19	116.36051	-38.19643	0.317	0.043	-0.025	7σ

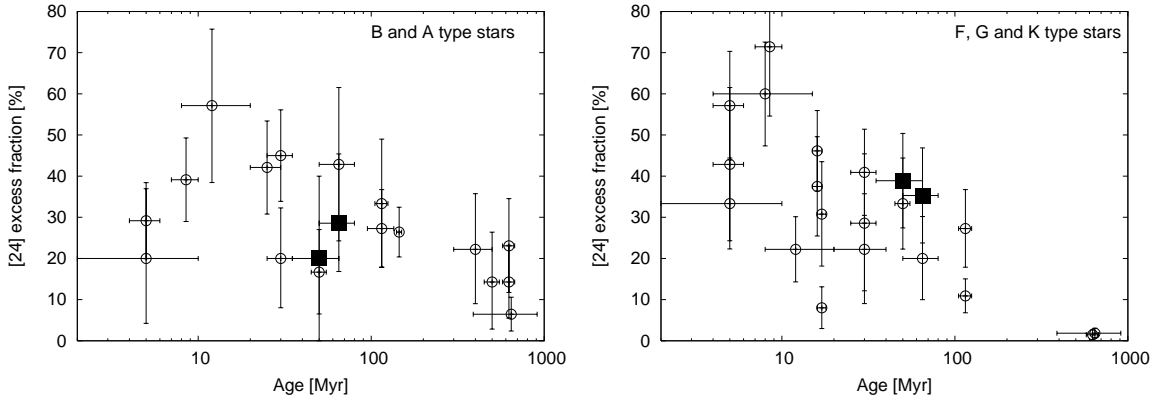


FIG. 15.— The fraction of star with $24\mu\text{m}$ excess vs age in open clusters. Left panel: early type stars. Right panel: solar type stars. Open circles: data from (Gáspár et al. 2009); filled squares: NGC2451 A and B

in Fig 12) in NGC2451 B and the three faintest ones (#7 and the two photospheric sources around $V-K \sim 3$ Fig 12 left panel) in NGC2451 A, the excess fractions ($35 \pm 12\%$ and $36 \pm 13\%$ for NGC2451 A and B, respectively) are still slightly above the main locus.

Unfortunately low number statistics might reduce the reliability of these results. To check whether they are statistically significant we binned the cluster data of Gáspár et al. (2009) supplemented with our two clusters into five equal logarithmic age bins 3-10 Myr, 10-31.6 Myr, 31.6-100 Myr, 100-316 Myr, 316-1000 Myr. We show the result of the binning in Fig 16 (left panel: early type stars; right panel: late type stars). There is a hint of a drop (about 1σ) in the excess fraction of early type stars in the 31.6-100 Myr range then, a rise and another drop after 316 Myr. For the late type stars a small bump breaks the continuous decay with about the same significance as the dip in the early type sample. More detailed and very accurate membership study of the clusters in this age range is necessary to decide whether this behavior can be attributed solely to statistical fluctuation.

5.2. Stars with large excess

Among all stars in NGC 2451 A/B showing excess at $24\mu\text{m}$, #12 (HD 62938) has by far the largest; $K-[24] = 1.6$ corresponding to an excess ratio (R) more than 4 meaning that the $24\mu\text{m}$ flux density is more the 4 times larger than the expected photospheric flux level. The MIPS data place a 2σ upper limit of 63 mJy on the flux density at $70\ \mu\text{m}$, requiring a color temperature between 24 and $70\ \mu\text{m} \geq 95\ \text{K}$. To put this star into context with other results we performed a literature search for main-sequence stars older than 20 Myr with similarly large or larger excess. We found 9 stars with excess ratios larger than 4 at $24\mu\text{m}$. We also included two famous somewhat younger large excess stars HD39060 (β Pic) and HD181296 (η Tel) for comparison. They are listed in Table 8. The excess of HD21362, a B6 star, is due to free-free emission so we rejected this star from our final sample.

Fig 17 shows the excess vs age diagram for our sample of 10 stars together with the sample of Rieke et al. (2005). We express the excess in $2.5 \times \log(R)$ so we can compare the Rieke et al. (2005) data with other publica-

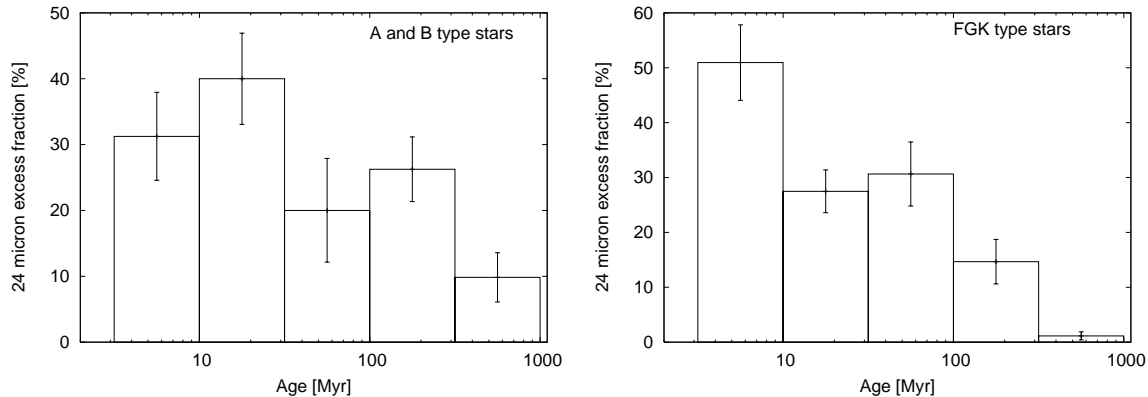


FIG. 16.— The binned excess fraction of open cluster vs age. Left panel: early type stars. Right panel: solar type stars.

TABLE 8
STARS WITH LARGE 24μ EXCESS

Name	SpT	Age	excess ref.	age ref
HD21362 [†]	B6Vn	80 Myr	Rieke et al. (2005)	Song et al. (2001)
HD39060	A5V	12 Myr	Rieke et al. (2005)	Ortega et al. (2002, 2004)
HD109573	A0V	10-20 Myr	Rieke et al. (2005)	Zuckerman & Song (2004a)
NSV17775 [‡]	A1V	25 Myr	Young et al. (2004)	Jeffries & Oliveira (2005)
NGC2547/id8	G7V	35 Myr	Gorlova et al. (2007)	Jeffries & Oliveira (2005)
NGC2547/id7	M	35 Myr	Gorlova et al. (2007)	Jeffries & Oliveira (2005)
P1121	F9V	80 Myr	Gorlova et al. (2004)	Rojo Arellano et al. (1997)
BD+20 307	G0	2 Gyr	Song et al. (2005)	Song et al. (2005)
HD23514	F6	120 Myr	Rhee et al. (2008)	Rhee et al. (2008)
HD181296	A0V	12 Myr	Su et al. (2006)	Zuckerman & Song (2004b)
HD62938 (#12)	A0V	50-80 Myr	this work	Platais et al. (2001)

[†] excess comes from free-free emission[‡] incorrectly listed as a Cataclysmic Variable Star in SIMBAD

tions where the excess is expressed in K-[24] mag. All but three of the stars with large excesses fall within the envelope of the decay trend of Rieke et al. (2005). (The normalization of this envelope is somewhat arbitrary so no distinction should be made between stars just above or just below it.) Two exceptions, P1121 of Gorlova et al. (2004) and HD23514 of Rhee et al. (2008), are young. The third one BD+20 307 (Song et al. 2005) is very old (about 2 Gyr (Zuckerman et al. 2008)). The excesses of these stars are much higher than would be predicted

based on their ages. Another two stars that are older than 30 Myr are borderline cases close to the upper envelope of the decay trend. One of them is a G7 star (ID8 in NGC 2547 Gorlova et al. (2007)) the other is an M star in the same cluster (ID7). We retain these two stars as candidate extreme excess stars.

Although these stars were identified only on the basis of their large excesses at $24\mu\text{m}$, they have a number of unique characteristics in comparison with other debris disks. For example, without full spectral energy distributions we cannot compute the fractional luminosities, L_d/L_* , but we can put lower limits on this parameter. As an illustration, we assume a star represented by a 6000K blackbody and a blackbody-like excess ten times the stellar output at $24\mu\text{m}$. The minimum fractional luminosity is then 2×10^{-3} at an excess temperature of between 150 and 160K. Seven of the ten large excess stars are at this level or above. The minimum fractional luminosity for the remaining three large excess sources is $\geq 2 \times 10^{-4}$. For comparison, debris disks typically have fractional luminosities below 10^{-4} (Moór et al. 2006). In addition, many of these systems are known to have strong spectral features in the mid-infrared, establishing that their emission there is dominated by warm, very finely divided dust (β Pic, Chen et al. (2007); NGC 2547 ID8 and P1121, Gorlova et al. in preparation; BD +20 307, Song et al. (2005); HD 23514, Rhee et al. (2008)).

These latter sources represent extreme examples of

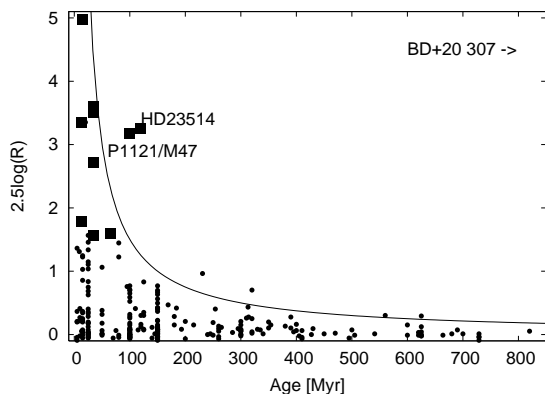


FIG. 17.— $24\mu\text{m}$ excess vs age. Squares: stars with large excess from Table 8, dots: stars from Rieke et al. (2005), solid line: the normal decay trend from infrared excesses

debris disks containing warm dust. Additional examples of systems with warm dust include Fomalhaut (Stapelfeldt et al. 2004); β Leo, (Akeson et al. 2009, our unpublished observations); η Tel, (Smith et al. 2009); η Corvi, (Smith et al. 2008); HR 4796A, (Wahhaj et al. 2005); ϵ Eri, (Backman et al. 2009); HD 113766, (Lisse et al. 2008); HD 69830, (Beichman et al. 2005); and ζ Lep, (Moerchen et al. 2007). Morales et al (2009) report 28 additional systems with dust at $T \geq 180$ K and that dominates the disk emission at 24μ . It is therefore plausible that many of the other large excess systems have substantial emission by warm dust.

Although many of the large-excess stars are roughly of solar type, even in this case they are relatively uncommon. In particular, for the 30 - 130 Myr age range, Table 8 shows there are only three solar-like extreme excess stars. They are drawn from a parent population of all the stars observed within this age range and with spectral types between mid-F (F4) and mid-K (K4), a total of about 250 (from M47, Gorlova et al. (2004); the Pleiades, Stauffer et al. (2005), Gorlova et al. (2006), and our unpublished work; IC 2391, Siegler et al. (2007); NGC 2547, Gorlova et al. (2007); the FEPS sample, Meyer et al. (2008); and NGC 2451A&B, this work). That is, the incidence of extreme excess systems among solar-like stars in the 30-130Myr age range is only about 1%.

The 30-130Myr age range insures that these extreme excesses are unlikely to originate in the wave of oligarth planet building that peaks around 10-15 Myr (e.g., Currie et al. (2008) and references therein). There are alternative possibilities for generating them, however. One is collisions between large bodies, similar to the collision that led to the formation of the Moon (Rhee et al. 2008). It is thought that about three moon masses of material were thrown into orbit around the Sun in the impact that formed our Moon (Canup 2004). The rapid injection of such a large mass would produce a signature roughly in agreement with the observations of these large-excess objects (Gorlova et al. in preparation). A rough e-folding time of 2 million years for the dissipation of this mass can be estimated from the calculations of Grogan et al. (2001). In addition, a process that results in very vigorous gravitational stirring of a dense asteroid belt (e.g., through gravitationally resonant orbits of massive planets, Gomes et al. (2005)) is also a candidate to produce huge infrared excesses.

Although Table 8 contains several early type stars older than 20 Myr and with large excesses, none of them is above the decay trend of normal debris disk stars. In fact, as Table 8 emphasizes, all the large-excess early type stars are relatively young and may just still be in the decay of their initial peak debris output. The placement of the trend line is rather arbitrary. Nevertheless, we have considered why no very large excesses are found for older early-type stars. We calculated what mass would be needed to cause an excess about 4 times above the stellar photosphere at $24 \mu\text{m}$ in an A star. We used only grains larger than $6.3 \mu\text{m}$, because radiation pressure will eject small grains from the system, with terminal velocity $v = \frac{2GM_\star}{r_{init}}(\beta - \frac{1}{2})^{\frac{1}{2}}$ where M_\star is the mass of the central star, r_{init} is the radius of the initial orbit of the grain and β is the ratio of forces from radiation pressure and grav-

ity. Dominik & Decin (2003) showed that the orbiting grains normally dominate the visibility of the debris disk over the blown-out grains. To get the total mass needed to cause the required $24\mu\text{m}$ excess we first assumed that all the flux comes from the smallest grains then we calculated the total surface area of these grains. Using the surface area and the $N(a) \sim a^{-3.5}$ grain size distribution we were able to determine the scaling constant using the following equation

$$\int_{a_{min}}^{a_{max}} 4\pi \frac{a^2}{4} ca^{-3.5} da = N_{a_{min}} 4\pi \frac{a_{min}^2}{4} \quad (6)$$

where a_{min} is the diameter of the smallest grain remaining in the system and a_{max} is a nominal maximum parent planetesimal size (100m). Using the scaling constant we can calculate the total mass by integrating $\frac{4}{3}\pi a^3 \rho ca^{-3.5}$ from a_{min} to a_{max} . We found that the total mass needed to produce the excess is on the order of a couple of Moon masses. The same calculation for G-type stars with $a_{min} = 0.01\mu\text{m}$ leads to two orders of magnitude less mass ($\sim 10^{-2}M_{Moon}$).

In the case of A stars, radiation pressure clears the small grains from the disk in a few hundred years while these grains remain around the G-star for a few times 10^4 years (Chen et al. 2005). To quantify the effects of this difference, we also calculated the scaling factor and the total mass neglecting the effect of blowout for the A star and integrating over the entire size range from $10^{-2}\mu\text{m}$ to 100m. We found that in this case we would need more than 25 times less material for producing the same level of excess around the A star. In this hypothetical case the masses needed for A- and G-type stars are the same order of magnitude. This implies that their ability to eject grains very efficiently through photon pressure plays a large role in the absence of extreme excess around older early type stars. Those small grains carry a large surface area (relative to their mass) which would make the excess more easily detectable. A corollary is that large grain production rates around early-type stars will be indicated by large flows of small grains out of the system driven by photon pressure. Possible examples include Vega (Su et al. 2005) and HR8799 (Su et al. in preparation)

6. CONCLUSIONS

We present optical and *Spitzer*/IRAC-MIPS photometry and medium resolution spectroscopy of the central 0.75 sq deg. region of NGC 2451 A and B. Using radial velocity data and optical/near-IR color magnitude diagrams we selected 61 members of NGC 2451 A and 131 members of NGC2451 B. We found one object in NGC2451 B and none in NGC2451 A with excess at $8\mu\text{m}$. We conclude that 8 micron excesses at the ages of these clusters are probably associated with an isolated event that disturbs the distribution of planetesimals to yield a sequence of collisional cascades producing dust.

We find one object with $24\mu\text{m}$ excess among the early type stars of NGC 2451 B and none in NGC2451 A. For the solar type stars we found 5 out of 15 stars with excess in NGC2451 A and 7 out of 16 for NGC2451 B. In general these results agree with excess fractions reported in the literature.

We used the data presented in Gáspár et al. (2009)

supplemented with our new datapoints to plot the excess fraction vs age, and found that the excess fraction unexpectedly drops in the range of 30-80Myr for early type stars while it slightly rises in the same age for late type stars. We tested our findings by binning the cluster data of Gáspár et al. (2009) into equal logarithmic age bins. The results are consistent with some structure but also indicate that the fluctuations may be statistical in nature.

We summarize the detections to date of large debris-disk 24 μm excesses. There are only five extreme cases, with fractional luminosities $\geq 2 \times 10^{-3}$. We did not find extreme excesses around older early type stars, excesses that would indicate a catastrophic collision between forming planetesimals. We found that blowout of the small

grains probably plays a very important role in the lack of detections.

We thank the anonymous referee for comments and suggestions that greatly improved the manuscript. This work is based on observations made with the Spitzer Space Telescope, which is operated by the Jet Propulsion Laboratory, California Institute of Technology, under NASA contract 1407. Support for this work was provided by NASA through contract 1255094, issued by JPL/Caltech. ZB also received support from Hungarian OTKA Grants T049082 and K76816. LLK has been supported by the Anglo-Australian Observatory and the Australian Research Council

REFERENCES

- Akeson, R. L., et al. 2009, *ApJ*, 691, 1896
 Andretta, V., Busà, I., Gomez, M. T., & Terranegra, L. 2005, *A&A*, 430, 669
 Beichman, C. A., et al. 2005, *ApJ*, 626, 1061
 Backman, D., et al. 2009, *ApJ*, 690, 1522
 Canup, R. M. 2004, *ARA&A*, 42, 441
 Chen, C. H., et al. 2005, *ApJ*, 634, 1372
 Chen, C. H., et al. 2007, *ApJ*, 666, 466
 Currie, T., Kenyon, S. J., Balog, Z., Rieke, G., Bragg, A., & Bromley, B. 2008, *ApJ*, 672, 558
 Dominik, C. & Decin, G. 2003, *ApJ*, 598, 626
 Fazio, G. G., et al. 2004, *ApJS*, 154, 10
 Gáspár, A., et al. 2009, *ApJ* accepted (arXiv:0903.4193)
 Gautier, T. N., III, et al. 2007, *ApJ*, 667, 527
 Gomes, R., Levison, H. F., Tsiganis, K., & Morbidelli, A. 2005, *Nature*, 435, 466
 Gordon, K. D., et al. 2005, *PASP*, 117, 503
 Gorlova, N., et al. 2004, *ApJS*, 154, 448
 Gorlova, N., Rieke, G. H., Muzerolle, J., Stauffer, J. R., Siegler, N., Young, E. T., & Stansberry, J. A. 2006, *ApJ*, 649, 1028
 Gorlova, N., Balog, Z., Rieke, G. H., Muzerolle, J., Su, K. Y. L., Ivanov, V. D., & Young, E. T. 2007, *ApJ*, 670, 516
 Grogan, K., Dermott, S. F., & Durda, D. D. 2001, *Icarus*, 152, 251
 Gutermuth, R. A., Megeath, S. T., Muzerolle, J., Allen, L. E., Pipher, J. L., Myers, P. C., & Fazio, G. G. 2004, *ApJS*, 154, 374
 Gutermuth, R. A., et al. 2008, *ApJ*, 674, 336
 Hünsch, M., Randich, S., Hempel, M., Weidner, C., & Schmitt, J. H. M. M. 2004, *A&A*, 418, 539
 Hünsch, M., Weidner, C., & Schmitt, J. H. M. M. 2003, *A&A*, 402, 571
 Jeffries, R. D., & Oliveira, J. M. 2005, *MNRAS*, 358, 13
 Kharchenko, N. V., Piskunov, A. E., Röser, S., Schilbach, E., & Scholz, R.-D. 2005, *A&A*, 438, 1163
 Kiss, L. L., Szabó, G. M., Balog, Z., Parker, Q. A., & Frew, D. J. 2008, *MNRAS*, 391, 399
 Kiss, L. L., Székely, P., Bedding, T. R., Bakos, G. Á., & Lewis, G. F. 2007, *ApJ*, 659, L129
 Landolt, A. U. 1992, *AJ*, 104, 340
 Lisse, C. M., Chen, C. H., Wyatt, M. C., & Morlok, A. 2008, *ApJ*, 673, 1106
 Meyer, M. R., et al. 2008, *ApJ*, 673, L181
 Rojo Arellano, E., Pena, J. H., & Gonzalez, D. 1997, *A&AS*, 123, 25
 Moerchen, M. M., Telesco, C. M., Packham, C., & Kehoe, T. J. J. 2007, *ApJ*, 655, L109
 Morales, F. Y., Werner, M. W., Bryden, G., Plavchan, P., Stapelfeldt, K. R., Rieke, G. H., Su, K. Y. L., Beichman, C. A., Chen, C. H., Grogan, K., Kenyon, S. J., Moro-Martín, A. & Wolf, S. 2009, *ApJ*, submitted
 Moór, A., Ábrahám, P., Derekas, A., Kiss, C., Kiss, L. L., Apai, D., Grady, C., & Henning, T. 2006, *ApJ*, 644, 525
 Munari, U., Sordo, R., Castelli, F., & Zwitter, T. 2005, *A&A*, 442, 1127
 Ortega, V. G., de la Reza, R., Jilinski, E., & Bazzanella, B. 2002, *ApJ*, 575, L75
 Ortega, V. G., de la Reza, R., Jilinski, E., & Bazzanella, B. 2004, *ApJ*, 609, 243
 Platais, I., Kozhurina-Platais, V., Barnes, S., Girard, T. M., Demarque, P., van Altena, W. F., Deliyannis, C. P., & Horch, E. 2001, *AJ*, 122, 1486
 Rhee, J. H., Song, I., & Zuckerman, B. 2007, *ApJ*, 671, 616
 Rhee, J. H., Song, I., & Zuckerman, B. 2008, *ApJ*, 675, 777
 Rieke, G. H., et al. 2005, *ApJ*, 620, 1010
 Rieke, G. H., et al. 2004, *ApJS*, 154, 25
 Siegler, N., Muzerolle, J., Young, E. T., Rieke, G. H., Mamajek, E. E., Trilling, D. E., Gorlova, N., & Su, K. Y. L. 2007, *ApJ*, 654, 580
 Siess, L., Dufour, E., & Forestini, M. 2000, *A&A*, 358, 593
 Smith, R., Wyatt, M. C., & Dent, W. R. F. 2008, *A&A*, 485, 897
 Smith, R., Churcher, L. J., Wyatt, M. C., Moerchen, M. M., & Telesco, C. M. 2009, *A&A*, 493, 299
 Song, I., Caillault, J.-P., Barrado y Navascués, D., & Stauffer, J. R. 2001, *ApJ*, 546, 352
 Song, I., Zuckerman, B., & Bessell, M. S. 2003, *ApJ*, 599, 342
 Song, I., Zuckerman, B., Weinberger, A. J., & Becklin, E. E. 2005, *Nature*, 436, 363
 Stapelfeldt, K. R., et al. 2004, *ApJS*, 154, 458
 Stauffer, J. R., et al. 2005, *AJ*, 130, 1834
 Steinmetz, M., et al. 2006, *AJ*, 132, 1645
 Su, K. Y. L., et al. 2005, *ApJ*, 628, 487
 Su, K. Y. L., et al. 2006, *ApJ*, 653, 675
 Touboul, M., Kleine, T., Bourdon, B., Palme, H., & Wieler, R. 2007, *Nature*, 450, 1206
 Trilling, D. E., et al. 2008, *ApJ*, 674, 1086
 Wahhaj, Z., Koerner, D. W., Backman, D. E., Werner, M. W., Serabyn, E., Ressler, M. E., & Lis, D. C. 2005, *ApJ*, 618, 385
 Young, E. T., et al. 2004, *ApJS*, 154, 428
 Zuckerman, B., & Song, I. 2004a, *ARA&A*, 42, 685
 Zuckerman, B., & Song, I. 2004b, *ApJ*, 603, 738
 Zuckerman, B., Fekel, F. C., Williamson, M. H., Henry, G. W., & Muno, M. P. 2008, *ApJ*, 688, 1345
 Zwitter, T., et al. 2008, *AJ*, 136, 421

TABLE 3
UBVR IJHK PHOTOMETRY OF THE MEMBERS OF NGC2451 A.

RA J2000	DEC J2000	U mag	$\sigma(U)$ mag	B mag	$\sigma(B)$ mag	V mag	$\sigma(V)$ mag	R mag	$\sigma(R)$ mag	I mag	$\sigma(I)$ mag	$\sigma(J)$ mag	J mag	H mag	$\sigma(H)$ mag	K mag	$\sigma(K)$ mag
115.72653	-37.99071	19.841	0.043	18.399	0.017	16.579	0.014	14.793	0.031	14.201	0.038	13.917	0.059
115.73360	-38.35236	19.495	0.035	17.700	0.016	15.724	0.012	13.626	0.032	13.061	0.034	12.712	...
115.75735	-37.70676	19.095	0.036	17.701	0.017	16.180	0.009	14.628	0.032	14.010	0.033	13.685	0.060
115.77562	-37.69178	18.338	0.017	16.937	0.020	15.265	0.009	13.666	0.031	13.076	0.028	12.782	0.032
115.77648	-38.15585	17.636	0.013	16.611	0.006	15.152	0.008	14.158	0.010	13.017	0.008	11.758	0.023	11.104	0.020	10.912	0.021
115.80866	-38.21898	18.941	0.023	17.641	0.008	16.050	0.006	14.443	0.037	13.792	0.044	13.537	0.043
115.82023	-38.04878	19.826	0.046	18.482	0.013	16.752	0.009	15.153	0.043	14.527	0.059	14.209	0.069
115.84371	-37.73632	19.111	0.034	17.840	0.013	16.603	0.007	15.135	0.006	13.700	0.026	13.046	0.020	12.732	0.028
115.86862	-38.29049	19.471	0.041	18.046	0.013	16.319	0.008	14.551	0.026	13.915	0.024	13.673	0.053
115.91156	-38.23518	11.778	0.001	11.450	0.002	10.997	0.004	10.730	0.005	10.479	0.011	10.008	0.023	9.822	0.024	9.740	0.019
115.91624	-37.72572	17.166	0.008	15.702	0.003	14.643	0.003	13.527	0.003	12.361	0.025	11.683	0.020	11.519	0.023
115.91917	-38.11346	20.360	0.079	18.858	0.020	17.086	0.013	15.353	0.052	14.720	0.063	14.374	0.080
115.95297	-38.36620	16.833	0.019	15.337	0.004	11.987	0.021	11.298	0.026	11.069	0.017
115.96202	-38.11860	17.641	0.013	16.123	0.015	14.972	0.011	13.504	0.016	11.965	0.028	11.340	0.027	11.104	0.023
115.97014	-38.27538	17.413	0.011	16.422	0.006	14.939	0.006	13.902	0.004	12.684	0.005	11.405	0.021	10.764	0.022	10.555	0.019
115.97250	-37.95827	19.721	0.045	18.392	0.015	16.773	0.014	15.282	0.057	14.755	0.072	14.051	0.100
115.97843	-37.77519	18.779	0.041	17.984	0.008	16.505	0.006	15.407	0.005	14.095	0.003	12.765	0.023	12.101	0.020	11.889	0.021
115.98955	-38.46418	14.697	0.002	13.537	0.002	11.286	0.023	10.671	0.024	10.562	0.019
116.03289	-37.84594	17.328	0.010	16.305	0.003	14.840	0.004	13.925	0.006	13.015	0.005	11.877	0.021	11.252	0.022	11.056	0.021
116.04942	-37.73994 (#6)	17.567	0.009	16.103	0.020	15.181	0.028	14.261	0.024	12.831	0.045	12.017	0.038	11.866	0.041
116.11263	-37.74447	20.063	0.054	18.823	0.023	17.052	0.008	15.400	0.051	14.774	0.059	14.391	0.088
116.13418	-37.68301	18.826	0.022	17.485	0.010	15.789	0.006	14.157	0.025	13.515	0.030	13.264	0.042
116.13475	-38.03229	11.692	0.003	11.622	0.005	10.985	0.004	10.634	0.008	10.246	0.008	9.714	0.021	9.446	0.022	9.351	0.019
116.14048	-38.15269	17.287	0.007	15.839	0.005	14.970	0.002	14.132	0.003	12.850	0.023	12.240	0.027	12.000	0.021
116.18760	-38.32344	19.484	0.058	17.932	0.010	16.059	0.005	14.209	0.025	13.675	0.026	13.351	0.038
116.20787	-38.16160	12.949	0.016	12.152	0.015	11.716	0.022	11.366	0.024	10.763	0.034	10.468	0.043	10.238	0.028
116.21219	-37.85936	13.672	0.002	13.310	0.002	12.486	0.001	12.072	0.005	11.673	0.004	11.109	0.025	10.751	0.030	10.650	0.024
116.21249	-37.74415	20.312	0.062	18.575	0.020	17.284	0.008	15.699	0.004	14.195	0.025	13.550	0.028	13.302	0.045
116.23017	-38.07956 (#9)	11.160	0.006	10.931	0.006	10.702	0.006	10.218	0.019	10.092	0.020	10.039	0.019
116.25277	-37.53289	15.244	0.004	14.176	0.004	12.228	0.023	11.699	0.022	11.605	0.021
116.25701	-38.03892	10.508	0.003	10.059	0.005	9.817	0.003	9.614	0.004	9.182	0.018	8.992	0.020	8.947	0.023
116.27029	-38.07462	19.862	0.057	19.186	0.029	17.688	0.012	16.439	0.005	14.910	0.004	13.260	0.025	12.667	0.028	12.444	0.029
116.28444	-38.14332	15.410	0.003	14.181	0.007	13.469	0.013	12.859	0.003	11.965	0.019	11.388	0.022	11.261	0.021
116.29981	-37.79209	19.561	0.023	18.039	0.015	16.775	0.005	15.178	0.006	13.617	0.026	12.985	0.024	12.749	0.032
116.31223	-38.19624 (#8)	10.882	0.007	10.905	0.003	10.424	0.007	10.155	0.006	9.874	0.008	9.467	0.058	9.249	0.077	9.192	0.062
116.33550	-37.89964	15.011	0.003	13.945	0.002	13.342	0.002	12.809	0.004	11.905	0.019	11.391	0.020	11.266	0.019
116.36404	-37.59628	6.857	0.002	6.909	0.001	7.045	0.013	7.086	0.021	7.101	0.005
116.38750	-37.51380	19.023	0.029	17.583	0.029	13.661	0.025	13.015	0.022	12.791	0.030
116.38871	-38.27644	19.821	0.026	18.180	0.013	16.889	0.005	15.241	0.004	13.574	0.021	12.951	0.024	12.632	0.030
116.38876	-38.13771	14.901	0.002	13.763	0.006	13.124	0.005	12.598	0.002	11.846	0.023	11.274	0.020	11.184	0.019
116.39985	-37.77279	19.578	0.025	17.903	0.013	16.586	0.007	14.889	0.010	13.296	0.019	12.747	0.020	12.462	0.017
116.43397	-37.73853	19.867	0.055	18.637	0.015	17.131	0.013	16.144	0.009	15.103	0.013	13.998	0.026	13.291	0.022	12.981	0.029
116.44578	-37.93944	18.874	0.026	17.368	0.005	15.594	0.004	13.805	0.021	13.244	0.026	12.952	0.030
116.47578	-37.86585	19.828	0.027	18.197	0.012	16.821	0.005	15.093	0.005	13.481	0.026	12.880	0.028	12.612	0.029
116.48650	-37.80289	19.659	0.036	18.265	0.010	16.487	0.010	14.780	0.037	14.180	0.037	13.918	0.062
116.53485	-37.89772	17.475	0.006	15.952	0.006	14.920	0.005	13.666	0.006	12.433	0.019	11.774	0.020	11.572	0.019
116.54976	-38.10431	19.566	0.025	18.019	0.013	14.567	0.013	14.982	0.022	13.412	0.021	12.819	0.020	12.577	0.024
116.56485	-38.46915	18.459	0.046	16.935	0.012	12.909	0.019	12.332	0.026	12.054	0.023
116.60356	-38.01960	14.299	0.005	13.646	0.004	12.703	0.004	10.098	0.008	11.770	0.008	11.083	0.019	10.655	0.022	10.568	0.019
116.61087	-38.08359	16.206	0.008	15.690	0.010	14.564	0.014	11.761	0.013	13.218	0.016	12.189	0.023	11.663	0.026	11.480	0.021
116.62418	-37.87896	19.176	0.016	17.618	0.008	16.359	0.007	14.725	0.004	13.161	0.023	12.573	0.028	12.319	0.023
116.70172	-38.14828	9.890	0.001	9.453	0.000	9.191	0.012	8.953	0.001	8.642	0.017	8.431	0.029	8.411	0.039
116.74747	-38.37820 (#7)	14.472	0.003	13.445	0.001	11.466	0.019	10.928	0.022	10.802	0.019
116.74952	-37.83876	19.006	0.018	18.121	0.007	16.602	0.005	15.521	0.004	14.177	0.004	12.934	0.023	12.344	0.022	12.074	0.021

TABLE 3 — *Continued*

RA J2000	DEC J2000	U mag	$\sigma(U)$ mag	B mag	$\sigma(B)$ mag	V mag	$\sigma(V)$ mag	R mag	$\sigma(R)$ mag	I mag	$\sigma(I)$ mag	$\sigma(J)$ mag	$\sigma(J)$ mag	H mag	$\sigma(H)$ mag	K mag	$\sigma(K)$ mag
116.76556	-37.95779	18.213	0.009	16.693	0.010	13.411	0.012	14.088	0.015	12.752	0.021	12.106	0.024	11.909	0.021
116.76661	-38.21130	17.462	0.052	17.865	0.013	16.360	0.007	15.242	0.003	13.862	0.003	12.592	0.025	11.968	0.022	11.740	0.021
116.77044	-38.22134	16.491	0.014	15.807	0.004	14.624	0.004	13.917	0.003	13.271	0.003	12.467	0.025	11.859	0.022	11.705	0.023
116.80532	-37.93312	16.750	0.016	15.238	0.006	12.384	0.021	11.736	0.020	11.527	0.023
116.87226	-37.88074	11.358	0.003	10.870	0.001	9.664	0.021	9.541	0.020	9.428	0.019
116.93404	-37.98419	12.585	0.002	11.860	0.002	10.580	0.021	10.204	0.020	10.109	0.021
Members from Platais et al. (2001)																	
115.92881	-38.20190	6.262	...	6.351	6.648	0.019	6.708	0.019	6.735	0.009
115.97642	-38.00076	13.632	0.002	13.150	0.003	12.309	0.002	11.373	0.010	10.817	0.021	10.385	0.020	10.296	0.019
116.14244	-37.94292	5.792	...	5.890	6.063	0.003	6.177	0.035	6.146	0.017
116.18701	-38.05376 (#12)	7.570	...	7.580	7.583	0.019	7.676	0.049	7.637	0.025
116.24871	-38.09417	8.458	...	8.304	7.929	0.005	7.869	0.027	7.805	0.019
116.54395	-37.93366	5.776	...	5.870	6.030	0.009	6.100	0.037	6.107	0.011
116.75196	-37.84372	13.013	0.045	11.898	0.061	11.366	0.066	10.795	0.073	10.469	0.021	10.018	0.024	9.951	0.024
Members from Hünsch et al. (2003)																	
116.02866	-37.98943	17.94	...	16.43	12.409	0.025	11.772	0.022	11.542	0.023
116.10025	-38.59977 (#11)	11.562	0.002	10.953	0.001	9.648	0.023	9.325	0.026	9.196	0.017
116.53718	-37.39910 (#10)	11.18	...	10.66	9.669	0.019	9.437	0.020	9.439	0.021

numbers next to the coordinates designate 24 μm excess sources from Table 7

TABLE 4
UBVR_IJHK PHOTOMETRY OF THE MEMBERS OF NGC2451 B

RA J2000	DEC J2000	U mag	$\sigma(U)$ mag	B mag	$\sigma(B)$ mag	V mag	$\sigma(V)$ mag	R mag	$\sigma(R)$ mag	I mag	$\sigma(I)$ mag	$\sigma(J)$ mag	$\sigma(J)$ mag	H mag	$\sigma(H)$ mag	K mag	$\sigma(K)$ mag
115.72778	-37.95026	16.698	0.014	15.763	0.005	14.607	0.010	13.908	0.020	13.281	0.025	12.465	0.018	11.919	0.020	11.773	0.019
115.75046	-37.79300	19.520	0.072	18.393	0.020	16.887	0.007	15.726	0.006	14.473	0.004	13.047	0.026	12.345	0.026	12.106	0.024
115.75243	-37.95836	13.070	0.009	12.958	0.004	12.332	0.008	11.940	0.013	11.542	0.019	11.140	0.025	10.794	0.020	10.757	0.023
115.77086	-37.81706	12.230	0.004	12.070	0.002	11.563	0.002	11.199	0.002	10.918	0.004	10.425	0.023	10.217	0.020	10.134	0.019
115.77200	-37.98902	18.918	0.042	17.743	0.009	16.189	0.007	15.040	0.009	13.623	0.012	12.358	0.025	11.774	0.020	11.533	0.023
115.79673	-38.09564	15.036	0.003	14.024	0.004	13.427	0.008	12.869	0.007	12.031	0.021	11.503	0.020	11.406	0.019
115.79724	-38.15298	17.356	0.012	16.408	0.005	15.099	0.007	14.359	0.008	13.644	0.008	12.551	0.023	11.965	0.020	11.772	0.017
115.80643	-37.79030	20.087	0.084	18.473	0.020	17.077	0.007	15.387	0.007	13.659	0.026	13.062	0.028	12.764	0.032
115.82157	-38.28752	20.142	0.066	18.634	0.016	17.547	0.015	16.400	0.013	15.002	0.059	14.347	0.075	14.100	0.073
115.82535	-37.76639	19.925	0.069	18.409	0.021	17.095	0.007	15.607	0.005	14.057	0.031	13.343	0.030	13.162	0.030
115.83157	-38.09364	14.138	0.004	13.923	0.004	13.163	0.005	12.720	0.010	12.272	0.026	11.676	0.028	11.297	0.032	11.069	0.024
115.85167	-37.93698	14.240	0.006	13.407	0.006	12.918	0.003	12.464	0.006	11.843	0.021	11.429	0.020	11.313	0.019
115.86620	-37.92305	19.519	0.034	18.000	0.013	16.808	0.008	15.371	0.009	13.967	0.028	13.296	0.020	13.097	0.037
115.86779	-37.94924	15.193	0.005	14.188	0.006	13.609	0.004	13.075	0.009	12.257	0.023	11.757	0.020	11.628	0.021
115.86904	-38.05129	19.969	0.053	18.345	0.016	17.246	0.008	16.020	0.009	14.782	0.031	14.020	0.026	13.803	0.059
115.86959	-37.94765	19.879	0.056	18.684	0.022	17.108	0.012	15.694	0.078	15.074	0.082	14.735	0.133
115.87277	-37.75060	7.850	0.014	7.614	0.029	7.436	0.049	7.589	0.016	7.510	0.015	7.495	0.029	7.454	0.015
115.87687	-38.35557	13.305	0.012	12.520	0.012	12.134	0.011	11.705	0.007	11.109	0.029	10.813	0.040	10.740	0.036
115.90090	-37.87689	20.297	0.093	18.762	0.021	17.461	0.009	15.961	0.006	14.444	0.040	13.765	0.020	13.513	0.043
115.91875	-38.14002	13.582	0.002	12.891	0.004	12.508	0.020	12.081	0.007	11.563	0.023	11.277	0.024	11.180	0.023
115.93221	-37.69007	14.352	0.004	13.544	0.001	13.051	0.005	12.620	0.003	11.985	0.023	11.600	0.020	11.544	0.021
115.94174	-37.91011	20.711	0.160	18.913	0.035	17.501	0.012	15.911	0.008	14.389	0.028	13.740	0.026	13.501	0.037

TABLE 4 — *Continued*

RA J2000	DEC J2000	U mag	$\sigma(U)$ mag	B mag	$\sigma(B)$ mag	V mag	$\sigma(V)$ mag	R mag	$\sigma(R)$ mag	I mag	$\sigma(I)$ mag	$\sigma(J)$ mag	$\sigma(J)$ mag	H mag	$\sigma(H)$ mag	K mag	$\sigma(K)$ mag
115.95562	-37.89574 (#14)	11.049	0.026	10.627	0.020	10.198	0.038	9.890	0.052	9.637	0.028	9.453	0.026	9.364	0.021
115.95767	-38.21386	17.695	0.011	16.570	0.006	15.366	0.006	14.657	0.006	13.991	0.006	13.079	0.025	12.512	0.026	12.358	0.026
115.96495	-38.22524	19.851	0.072	18.476	0.019	16.991	0.009	16.088	0.008	15.288	0.007	14.262	0.035	13.533	0.026	13.372	0.041
115.98142	-38.18655	14.021	0.006	13.747	0.006	13.045	0.008	12.582	0.011	12.176	0.006	11.590	0.021	11.303	0.022	11.194	0.017
115.98473	-37.77708	19.327	0.063	18.293	0.012	16.733	0.006	15.663	0.007	14.491	0.005	13.084	0.031	12.404	0.028	12.169	0.028
115.99301	-37.62355	12.443	0.001	11.826	0.001	10.579	0.023	10.257	0.020	10.186	0.021
116.01189	-38.12175	18.681	0.018	17.096	0.011	16.040	0.006	14.866	0.007	13.479	0.031	12.868	0.030	12.606	0.033
116.01443	-38.12092	20.111	0.049	18.615	0.024	17.378	0.008	15.829	0.007	14.212	0.031	13.537	0.027	13.251	0.036
116.03135	-37.74863	18.849	0.023	17.565	0.009	15.938	0.005	14.295	0.050	13.631	0.053	13.364	0.053
116.04131	-37.91467	14.189	0.003	13.396	0.006	12.930	0.007	12.471	0.005	11.758	0.021	11.289	0.020	11.217	0.023
116.06585	-37.76541	18.603	0.030	17.563	0.007	16.150	0.005	15.204	0.005	14.188	0.004	12.885	0.028	12.175	0.024	11.975	0.021
116.08724	-37.88116	18.700	0.019	17.140	0.009	16.049	0.008	14.826	0.005	13.418	0.026	12.737	0.027	12.524	0.026
116.09396	-37.88209	13.915	0.002	13.148	0.003	12.725	0.005	12.293	0.004	11.741	0.023	11.305	0.022	11.222	0.021
116.09680	-37.92455	11.746	0.003	11.841	0.002	11.381	0.004	11.150	0.004	10.856	0.006	10.502	0.021	10.289	0.022	10.263	0.021
116.12193	-37.77896	13.539	0.002	13.459	0.002	12.780	0.002	12.387	0.004	11.989	0.005	11.383	0.021	11.070	0.022	10.962	0.021
116.13069	-37.72335	18.664	0.014	17.185	0.006	16.228	0.005	15.360	0.006	14.286	0.031	13.579	0.035	13.422	0.042
116.13331	-37.74069	19.974	0.048	18.337	0.019	17.243	0.009	15.967	0.006	14.625	0.051	13.890	0.073	13.608	0.068
116.15142	-37.81565	19.207	0.040	18.199	0.011	16.677	0.006	15.653	0.005	14.485	0.005	13.120	0.040	12.450	0.035	12.259	0.043
116.15163	-37.90051	14.245	0.001	13.444	0.003	12.994	0.004	12.520	0.004	11.763	0.021	11.352	0.026	11.258	0.021
116.15218	-38.40723	14.863	0.015	13.887	0.005	12.080	0.021	11.645	0.022	11.568	0.019
116.15345	-37.91661	18.553	0.026	17.112	0.008	16.043	0.018	14.884	0.012	13.600	0.029	12.915	0.029	12.729	0.028
116.15422	-37.82180	18.934	0.035	17.845	0.007	16.376	0.006	15.431	0.005	14.450	0.004	13.241	0.023	12.513	0.024	12.341	0.026
116.16007	-37.86702	20.366	0.078	19.004	0.022	17.164	0.007	15.290	0.069	14.694	0.063	14.309	0.094
116.17784	-38.18400	14.696	0.002	13.795	0.004	13.260	0.004	12.730	0.004	11.969	0.026	11.496	0.030	11.342	0.026
116.17909	-37.68557	20.267	0.065	18.728	0.019	16.843	0.007	14.997	0.039	14.415	0.053	14.073	0.070
116.18128	-38.30692	18.738	0.020	17.199	0.009	16.134	0.004	14.930	0.003	13.637	0.023	12.928	0.020	12.725	0.023
116.18606	-37.80272	19.693	0.032	18.154	0.014	16.907	0.007	15.350	0.005	13.776	0.026	13.143	0.027	12.945	0.026
116.20740	-38.13024	11.720	0.003	11.275	0.004	11.020	0.005	10.762	0.012	10.233	0.023	10.068	0.020	9.996	0.019
116.20831	-38.33110	19.185	0.026	17.662	0.020	16.496	0.019	15.237	0.012	13.803	0.028	13.110	0.028	12.886	0.032
116.21406	-38.13371	14.704	0.003	13.768	0.006	13.231	0.005	12.751	0.007	11.856	0.019	11.459	0.020	11.347	0.024
116.21574	-38.16710	19.726	0.055	18.489	0.022	16.936	0.030	15.945	0.022	14.961	0.028	13.775	0.029	13.106	0.030	12.956	0.036
116.21670	-38.28414	16.030	0.005	14.849	0.005	14.137	0.005	13.389	0.005	12.269	0.028	11.687	0.033	11.477	0.026
116.21722	-38.06004	17.118	0.012	16.667	0.006	15.410	0.011	14.652	0.008	13.954	0.012	12.774	0.023	12.193	0.022	12.047	0.021
116.21815	-37.99622	18.349	0.019	17.290	0.007	15.858	0.006	14.960	0.004	14.178	0.003	13.028	0.021	12.346	0.022	12.220	0.019
116.21956	-37.96960	20.921	0.117	19.227	0.036	17.869	0.011	16.202	0.007	14.504	0.052	13.888	0.059	13.410	0.059
116.23083	-37.78915	19.335	0.037	18.055	0.009	16.423	0.008	14.814	0.038	14.209	0.053	13.917	0.058
116.24108	-38.02993	19.110	0.027	17.808	0.007	16.264	0.006	14.616	0.018	13.966	0.032	13.616	0.046
116.26111	-38.03118	13.142	0.003	13.184	0.002	12.495	0.004	12.098	0.002	11.744	0.003	11.108	0.018	10.769	0.020	10.723	0.023
116.26560	-38.10297	13.505	0.003	12.782	0.004	12.392	0.002	12.035	0.002	11.356	0.019	11.037	0.022	10.976	0.019
116.26915	-37.94337	17.773	0.012	16.810	0.006	15.422	0.005	14.534	0.004	13.629	0.003	12.255	...	11.641	...	11.512	0.023
116.27896	-38.20475	18.211	0.015	17.283	0.005	15.938	0.006	15.080	0.004	14.235	0.003	13.085	0.021	12.392	0.026	12.241	0.019
116.28159	-37.66232	14.090	0.053	13.371	0.018	11.957	0.019	11.619	0.026	11.505	0.019
116.28564	-38.28589	20.188	0.040	18.509	0.017	17.233	0.006	15.617	0.004	14.031	0.026	13.333	0.028	13.068	0.037
116.29492	-38.32831	19.728	0.029	18.174	0.014	17.200	0.006	16.190	0.005	14.938	0.043	14.199	0.050	14.013	0.063
116.30032	-37.75469	14.114	0.003	13.927	0.004	13.211	0.007	12.784	0.004	12.379	0.009	11.764	0.021	11.378	0.022	11.273	0.019
116.30482	-37.83787	12.816	0.010	12.822	0.005	12.347	0.009	12.032	0.010	11.700	0.017	11.248	0.021	11.045	0.024	10.980	0.021
116.30806	-37.78869	19.309	0.018	17.744	0.010	16.617	0.004	15.276	0.006	13.931	0.021	13.242	0.028	12.984	0.032
116.32416	-37.81474	13.744	0.002	13.632	0.002	12.967	0.004	12.577	0.003	12.180	0.004	11.639	0.023	11.323	0.024	11.245	0.021
116.32484	-37.82308	14.232	0.002	14.233	0.002	13.619	0.005	13.232	0.004	12.816	0.004	12.212	0.021	11.843	0.028	11.793	0.026
116.33729	-37.83136	12.353	0.006	12.406	0.004	11.840	0.004	11.511	0.006	11.169	0.006	10.664	0.019	10.421	0.020	10.369	0.017
116.34253	-38.16618	19.725	0.023	18.063	0.016	16.754	0.005	15.107	0.006	13.446	0.023	12.784	0.020	12.541	0.024
116.34356	-38.06953	19.271	0.034	17.979	0.008	16.426	0.006	14.731	0.032	14.053	0.035	13.801	0.047
116.36942	-38.19338	19.282	0.028	17.863	0.027	16.246	0.014	14.559	0.036	13.909	0.043	13.589	0.049
116.37029	-38.09812	18.904	0.023	17.558	0.006	16.015	0.004	14.265	0.073	13.621	0.037	13.394	0.038
116.38677	-37.85640	20.094	0.053	19.315	0.021	17.737	0.011	16.477	0.005	14.919	0.008	13.355	0.019	12.682	0.020	12.469	0.023

TABLE 4 — *Continued*

RA J2000	DEC J2000	U mag	$\sigma(U)$ mag	B mag	$\sigma(B)$ mag	V mag	$\sigma(V)$ mag	R mag	$\sigma(R)$ mag	I mag	$\sigma(I)$ mag	$\sigma(J)$ mag	$\sigma(J)$ mag	H mag	$\sigma(H)$ mag	K mag	$\sigma(K)$ mag
116.39377	-37.86470	14.490	0.004	14.222	0.003	13.383	0.005	12.921	0.003	12.463	0.005	11.771	0.023	11.374	0.024	11.306	0.024
116.39548	-37.83491	19.610	0.040	18.156	0.012	16.334	0.010	14.581	0.034	13.920	0.033	13.691	0.053
116.39838	-37.91670	17.080	0.009	15.976	0.005	14.829	0.004	13.412	0.025	12.716	0.026	12.491	0.021
116.40154	-37.77890	17.754	0.010	16.632	0.009	15.334	0.009	14.551	0.006	13.831	0.005	12.797	0.023	12.152	0.028	11.983	0.026
116.40282	-37.94396	18.582	0.022	17.336	0.006	15.917	0.006	14.385	0.026	13.648	0.024	13.443	0.049
116.40669	-37.50750	13.859	0.002	13.084	0.002	11.479	0.021	11.058	0.026	10.960	0.024
116.44107	-37.89720 (#17)	14.167	0.002	13.360	0.004	12.872	0.002	12.314	0.004	11.465	0.018	11.027	0.020	10.877	0.017
116.45256	-37.54667	9.207	0.005	9.168	0.002	9.041	0.017	9.082	0.022	9.053	0.021
116.46779	-38.52593	16.118	0.009	14.950	0.003	12.619	0.018	12.004	0.022	11.854	0.024
116.48573	-37.95175	19.160	0.037	17.852	0.007	16.218	0.006	14.517	0.035	13.879	0.030	13.625	0.050
116.49277	-37.99629	13.171	0.022	12.993	0.010	12.222	0.013	9.650	0.022	11.268	0.029	10.782	0.023	10.409	0.020	10.365	0.023
116.50293	-37.67097	12.724	0.001	12.195	0.001	11.125	0.025	10.891	0.024	10.836	0.023
116.50903	-37.86043	15.997	0.006	14.849	0.004	13.677	0.005	13.051	0.003	12.476	0.003	11.578	0.019	11.117	0.020	10.943	0.023
116.50935	-38.07950	20.780	0.038	18.979	0.014	15.439	0.012	15.813	0.022	14.048	0.026	13.412	0.035	13.081	0.035
116.51448	-38.01421	20.828	0.047	19.171	0.016	15.728	0.008	16.250	0.017	14.674	0.038	14.036	0.041	13.745	0.056
116.54938	-38.21002	14.470	0.002	14.198	0.006	13.407	0.004	12.938	0.006	12.508	0.006	11.839	0.031	11.466	0.040	11.329	0.034
116.56459	-37.74740	19.043	0.020	17.928	0.015	16.468	0.009	15.515	0.009	14.495	0.011	13.272	0.021	12.571	0.020	12.394	0.021
116.57994	-37.56290	15.891	0.029	14.770	0.009	12.561	0.023	12.097	0.020	11.935	0.019
116.58564	-37.96366	19.706	0.020	16.238	0.009	16.659	0.010	15.028	0.044	14.374	0.050	14.068	0.073
116.60560	-38.23373	18.975	0.050	17.921	0.025	16.514	0.011	15.175	0.038	14.511	0.065	14.264	0.088
116.61145	-38.10934	19.886	0.023	18.104	0.011	14.648	0.010	15.220	0.012	13.468	0.018	12.752	0.024	12.459	0.019
116.66325	-38.32594	18.903	0.054	17.660	0.014	16.083	0.009	14.518	0.029	13.846	0.040	13.628	0.059
116.66850	-38.04359	19.475	0.021	18.212	0.006	16.620	0.010	13.479	0.013	14.611	0.017	13.315	0.065	12.531	0.064	12.379	0.053
116.67281	-37.84615	19.480	0.027	18.350	0.009	16.828	0.006	15.833	0.004	14.808	0.003	13.668	0.021	13.016	0.026	12.816	0.028
116.67488	-37.98390 (#13)	20.007	0.033	18.738	0.010	17.101	0.009	13.842	0.014	14.785	0.016	13.369	0.023	12.609	0.022	12.393	0.024
116.68185	-38.28975	15.533	0.006	14.996	0.004	14.056	0.005	13.520	0.003	13.026	0.004	12.251	0.019	11.816	0.022	11.744	0.024
116.68972	-37.82607	13.385	0.002	13.275	0.002	12.637	0.003	12.264	0.004	11.893	0.003	11.405	0.018	11.138	0.022	11.058	0.019
116.69822	-38.00890	19.840	0.025	16.320	0.018	16.685	0.023	14.974	0.036	14.231	0.046	13.991	0.068
116.72084	-37.71950	19.244	0.021	18.233	0.009	16.714	0.004	15.530	0.003	14.014	0.003	12.712	0.019	12.109	0.024	11.870	0.017
116.72728	-37.59192	16.163	0.015	14.964	0.005	12.630	0.021	12.037	0.020	11.893	0.021
116.73331	-38.35595	10.554	0.009	10.117	0.001	9.896	0.012	9.626	0.002	9.289	0.019	9.142	0.020	9.099	0.021
116.74249	-37.63916 (#18)	12.272	0.001	11.835	0.001	10.836	0.018	10.635	0.020	10.611	0.017
116.75339	-37.96264	19.255	0.017	15.751	0.012	16.204	0.013	14.627	0.045	13.833	0.041	13.556	0.060
116.76585	-37.96487	19.078	0.013	17.349	0.010	14.052	0.011	14.943	0.014	13.536	0.032	12.727	0.032	12.500	0.035
116.77636	-37.73380	18.212	0.012	17.143	0.009	15.735	0.007	14.843	0.008	13.970	0.009	13.062	0.025	12.362	0.020	12.231	0.024
116.79779	-37.79682	12.978	0.002	12.437	0.002	11.274	0.023	11.046	0.022	10.968	0.023
116.81857	-38.30363	11.909	0.001	11.437	0.001	10.414	0.019	10.210	0.022	10.147	0.019
116.84155	-38.30055	16.654	0.017	15.407	0.006	12.872	0.023	12.254	0.024	12.108	0.026
116.84765	-37.71917	15.081	0.012	13.926	0.004	11.711	0.024	11.226	0.036	11.080	0.026
116.86294	-38.13213	18.606	0.080	17.172	0.022	14.602	0.039	13.932	0.036	13.774	0.050
116.92513	-38.18621	15.655	0.003	14.615	0.003	12.534	0.037	12.030	0.049	11.857	0.035
116.94233	-38.15534	13.326	0.001	12.727	0.001	11.461	0.021	11.158	0.020	11.128	0.021
116.94269	-37.51560	15.373	0.044	14.468	0.014	12.659	0.021	12.193	0.022	12.105	0.024
116.94462	-37.88126	10.917	0.002	10.434	0.001	9.522	0.019	9.330	0.025	9.228	0.019
Members from Hünsch et al. (2003)																	
115.95710	-37.96688	10.025	0.001	9.855	0.001	9.736	0.009	9.682	0.013	9.547	0.023	9.511	0.020	9.470	0.019
116.03583	-37.98349	9.346	0.001	9.466	0.001	9.359	0.001	9.386	0.004	9.291	0.005	9.132	0.031	9.082	0.020	9.050	0.023
116.07976	-38.00541	15.48	...	14.37	12.076	0.023	11.508	0.022	11.362	0.017
116.15953	-38.22106	10.70	...	10.50	9.239	0.023	9.083	0.024	8.993	0.017
116.20300	-38.09869	14.24	...	13.49	11.899	0.019	11.478	0.024	11.410	0.023
116.21267	-37.66869 (#15)	10.99	...	10.70	10.022	0.019	9.898	0.022	9.797	0.023
116.36051	-38.19643 (#19)	12.030	0.009	11.997	0.002	11.438	0.005	11.137	0.004	10.816	0.004	10.366	0.026	10.095	0.022	10.037	0.021
116.38235	-37.50727	13.43	...	12.73	11.327	0.025	10.983	0.033	10.876	0.028

TABLE 4 — *Continued*

RA J2000	DEC J2000	U mag	σ (U) mag	B mag	σ (B) mag	V mag	σ (V) mag	R mag	σ (R) mag	I mag	σ (I) mag	σ (J) mag	σ (J) mag	H mag	σ (H) mag	K mag	σ (K) mag
116.39170	-37.79194	13.020	0.003	12.996	0.005	12.425	0.007	12.112	0.004	11.784	0.005	11.310	0.019	11.073	0.022	11.020	0.021
116.50776	-38.00752 (#16)	12.613	0.001	12.723	0.002	12.041	0.003	11.696	0.001	11.384	0.002	10.863	0.021	10.606	0.022	10.515	0.019

numbers next to the coordinates designate 24 μ m excess sources from Table 7

TABLE 5
Spitzer 3.6 μ m - 24 μ m PHOTOMETRY OF MEMBERS OF NGC2451 A

RA J2000	DEC J2000	[3.6] mag	σ ([3.6]) mag	[4.5] mag	σ ([4.5]) mag	[5.8] mag	σ ([5.8]) mag	[8.0] mag	σ ([8.0]) mag	[24] mag	σ ([24]) mag
115.72653	-37.99071
115.73360	-38.35236
115.75735	-37.70676
115.77562	-37.69178
115.77648	-38.15585
115.80866	-38.21898
115.82023	-38.04878
115.84371	-37.73632
115.86862	-38.29049
115.91156	-38.23518
115.91624	-37.72572	11.362	0.004	11.394	0.005	11.296	0.014	11.301	0.020
115.91917	-38.11346	14.216	0.014	14.111	0.021	14.038	0.096	13.916	0.147
115.95297	-38.36620	10.988	0.004	10.938	0.011
115.96202	-38.11860	10.906	0.004	10.868	0.004	10.822	0.010	10.830	0.014	10.489	0.055
115.97014	-38.27538	10.380	0.003	10.379	0.003	10.363	0.008	10.309	0.008
115.97250	-37.95827	14.134	0.014	14.086	0.023	14.559	0.128
115.97843	-37.77519	11.722	0.005	11.684	0.006	11.675	0.016	11.597	0.019
115.98955	-38.46418	10.401	0.054
116.03289	-37.84594	10.944	0.003	10.939	0.004	10.819	0.010	10.849	0.013
116.04942	-37.73994 (#6)	11.616	0.005	11.581	0.005	11.497	0.016	11.527	0.021	10.767	0.073
116.11263	-37.74447	14.175	0.015	14.081	0.022	13.986	0.102	13.812	0.124
116.13418	-37.68301	13.068	0.008	12.948	0.011	12.971	0.044	12.976	0.062
116.13475	-38.03229	9.382	0.002	9.403	0.003	9.374	0.005	9.365	0.005	9.245	0.034
116.14048	-38.15269	11.922	0.005	11.950	0.007	11.881	0.022	11.828	0.035
116.18760	-38.32344	13.070	0.008	12.990	0.046
116.20787	-38.16160	10.252	0.003	10.205	0.003	10.222	0.007	10.180	0.008	10.161	0.051
116.21219	-37.85936	10.638	0.003	10.695	0.004	10.671	0.009	10.647	0.014	10.708	0.067
116.21249	-37.74415	13.037	0.009	12.987	0.010	12.916	0.047	12.941	0.061
116.23017	-38.07956 (#9)	10.033	0.003	9.995	0.003	10.038	0.007	9.963	0.007	9.465	0.036
116.25277	-37.53289
116.25701	-38.03892	8.970	0.002	8.981	0.003	8.914	0.005	9.039	0.005	9.012	0.033
116.27029	-38.07462	12.226	0.007	12.145	0.008	12.139	0.022	12.110	0.041
116.28444	-38.14332	11.223	0.004	11.278	0.005	11.199	0.012	11.210	0.018	11.209	0.141
116.29981	-37.79209	12.534	0.006	12.477	0.008	12.413	0.027	12.439	0.039
116.31223	-38.19624 (#8)	9.193	0.003	9.162	0.004	9.136	0.005	9.137	0.004	8.645	0.046
116.33550	-37.89964	11.210	0.004	11.219	0.005	11.138	0.023	11.135	0.014
116.36404	-37.59628	7.220	0.002	7.189	0.002	7.230	0.031
116.38750	-37.51380
116.38871	-38.27644	12.409	0.006	12.271	0.027
116.38876	-38.13771	11.174	0.004	11.205	0.005	11.210	0.013	11.179	0.018
116.39985	-37.77279	12.182	0.005	12.145	0.007	12.004	0.021	12.057	0.033

TABLE 6 — *Continued*

RA J2000	DEC J2000	[3.6] mag	σ ([3.6]) mag	[4.5] mag	σ ([4.5]) mag	[5.8] mag	σ ([5.8]) mag	[8.0] mag	σ ([8.0]) mag	[24] mag	σ ([24]) mag
115.82535	-37.76639
115.83157	-38.09364
115.85167	-37.93698
115.86620	-37.92305
115.86779	-37.94924
115.86904	-38.05129
115.86959	-37.94765
115.87277	-37.75060	7.541	0.002	7.547	0.002	7.515	0.002	7.563	0.002
115.87687	-38.35557
115.90090	-37.87689	13.309	0.009	13.271	0.012	13.328	0.047	13.257	0.089
115.91875	-38.14002	11.166	0.003	11.186	0.004	11.152	0.013	11.213	0.016
115.93221	-37.69007	11.534	0.005	11.488	0.020
115.94174	-37.91011	13.250	0.010	13.170	0.012	13.205	0.047	13.166	0.054
115.95562	-37.89574 (#14)	9.343	0.002	9.373	0.003	9.310	0.005	9.308	0.004	8.549	0.034
115.95767	-38.21386	12.271	0.005	12.329	0.007	12.285	0.025	12.284	0.039
115.96495	-38.22524	13.292	0.009	13.379	0.013	13.277	0.048	13.476	0.086
115.98142	-38.18655	11.225	0.004	11.204	0.005	11.237	0.013	11.165	0.016
115.98473	-37.77708	12.048	0.006	12.052	0.007	11.980	0.021	11.922	0.033
115.99301	-37.62355	10.193	0.003	10.141	0.009	10.300	0.048
116.01189	-38.12175	12.425	0.007	12.425	0.009	12.372	0.025	12.417	0.043
116.01443	-38.12092	13.103	0.008	13.044	0.014	12.937	0.032	13.123	0.073
116.03135	-37.74863	13.200	0.009	13.131	0.013	12.974	0.040	13.169	0.088
116.04131	-37.91467	11.110	0.004	11.071	0.004	11.042	0.011	11.066	0.015
116.06585	-37.76541	11.889	0.005	11.840	0.006	11.798	0.016	11.778	0.032
116.08724	-37.88116	12.359	0.006	12.348	0.007	12.303	0.025	12.307	0.039
116.09396	-37.88209	11.148	0.004	11.183	0.005	11.116	0.012	11.132	0.018
116.09680	-37.92455	10.259	0.003	10.334	0.004	10.236	0.008	10.210	0.008	10.229	0.062
116.12193	-37.77896	10.950	0.003	10.973	0.004	10.929	0.011	10.903	0.014
116.13069	-37.72335	13.300	0.009	13.337	0.012	13.171	0.044	13.421	0.081
116.13331	-37.74069	13.008	0.025	12.923	0.034	12.936	0.078	12.797	0.065
116.15142	-37.81565	12.066	0.005	12.044	0.007	12.059	0.024	11.992	0.036
116.15163	-37.90051	11.229	0.004	11.224	0.005	11.138	0.014	11.184	0.014
116.15218	-38.40723	11.502	0.004	11.435	0.016
116.15345	-37.91661	12.568	0.007	12.576	0.009	12.383	0.024	12.582	0.047
116.15422	-37.82180	12.238	0.006	12.215	0.007	12.116	0.023	12.206	0.046
116.16007	-37.86702	14.124	0.015	14.029	0.019	14.097	0.088
116.17784	-38.18400	11.244	0.004	11.278	0.005	11.233	0.013	11.279	0.016
116.17909	-37.68557	13.816	0.012	13.784	0.015	13.806	0.076	13.748	0.119
116.18128	-38.30692	12.564	0.006	12.451	0.028
116.18606	-37.80272	12.694	0.007	12.653	0.008	12.619	0.031	12.696	0.046
116.20740	-38.13024	9.980	0.002	9.911	0.003	9.925	0.007	9.908	0.007	9.932	0.042
116.20831	-38.33110	12.683	0.007	12.591	0.034
116.21406	-38.13371	11.306	0.004	11.252	0.005	11.251	0.014	11.249	0.016
116.21574	-38.16710	12.728	0.007	12.709	0.009	12.663	0.032	12.553	0.048
116.21670	-38.28414	11.407	0.004	11.406	0.005	11.324	0.013	11.374	0.017
116.21722	-38.06004	11.936	0.005	11.940	0.006	11.905	0.022	11.927	0.049
116.21815	-37.99622	12.130	0.008	12.150	0.008	12.090	0.034	12.054	0.050
116.21956	-37.96960	13.577	0.027	13.396	0.017	13.642	0.130
116.23083	-37.78915	13.732	0.011	13.670	0.017	13.632	0.084	13.783	0.126
116.24108	-38.02993	13.476	0.016	13.386	0.023	13.265	0.051
116.26111	-38.03118	10.668	0.004	10.707	0.004	10.687	0.014	10.628	0.038
116.26560	-38.10297	10.927	0.003	10.948	0.004	10.889	0.011	10.936	0.013
116.26915	-37.94337	11.415	0.006	11.381	0.032	11.323	0.031	11.344	0.040
116.27896	-38.20475	12.141	0.005	12.104	0.007	12.039	0.021	12.041	0.036
116.28159	-37.66232	11.530	0.004	11.485	0.005	11.555	0.017	11.457	0.026

TABLE 6 — *Continued*

RA J2000	DEC J2000	[3.6] mag	σ ([3.6]) mag	[4.5] mag	σ ([4.5]) mag	[5.8] mag	σ ([5.8]) mag	[8.0] mag	σ ([8.0]) mag	[24] mag	σ ([24]) mag
116.28564	-38.28589	12.848	0.007	12.711	0.032
116.29492	-38.32831	13.914	0.014	13.883	0.087
116.30032	-37.75469	11.290	0.004	11.319	0.005	11.398	0.014	11.271	0.018
116.30482	-37.83787	10.996	0.003	10.998	0.004	11.039	0.012	10.957	0.016
116.30806	-37.78869	12.918	0.008	12.807	0.009	12.701	0.032	12.839	0.045
116.32416	-37.81474	11.223	0.004	11.257	0.005	11.217	0.013	11.241	0.019
116.32484	-37.82308	11.778	0.005	11.802	0.006	11.777	0.017	11.725	0.024
116.33729	-37.83136	10.373	0.003	10.353	0.003	10.383	0.008	10.319	0.008	10.624	0.066
116.34253	-38.16618	12.272	0.006	12.273	0.007	12.169	0.023	12.144	0.035
116.34356	-38.06953	13.550	0.010	13.512	0.014	13.515	0.081	13.531	0.100
116.36942	-38.19338	13.407	0.009	13.342	0.012	13.361	0.057	13.269	0.077
116.37029	-38.09812	12.924	0.008	12.995	0.011	13.111	0.064	12.889	0.049
116.38677	-37.85640	12.246	0.005	12.193	0.007	12.095	0.019	12.194	0.048
116.39377	-37.86470	11.217	0.004	11.271	0.005	11.270	0.014	11.227	0.014
116.39548	-37.83491	13.450	0.012	13.252	0.012	13.283	0.056	13.254	0.086
116.39838	-37.91670	12.237	0.007	12.423	0.012	12.508	0.093
116.40154	-37.77890	11.915	0.005	11.944	0.006	11.837	0.018	11.981	0.029
116.40282	-37.94396	13.175	0.008	13.212	0.013	13.662	0.077	13.289	0.082
116.40669	-37.50750
116.44107	-37.89720 (#17)	10.869	0.003	10.849	0.004	10.871	0.011	10.733	0.012	10.368	0.049
116.45256	-37.54667	9.088	0.003	9.057	0.004	8.977	0.038
116.46779	-38.52593
116.48573	-37.95175	13.559	0.010	13.329	0.013	13.270	0.054	13.560	0.088
116.49277	-37.99629	10.329	0.003	10.338	0.003	10.336	0.008	10.311	0.009	10.326	0.062
116.50293	-37.67097	10.801	0.003	10.819	0.004	10.805	0.010	10.725	0.013
116.50903	-37.86043	10.913	0.003	10.987	0.004	10.915	0.011	10.879	0.014
116.50935	-38.07950	12.816	0.007	12.745	0.009	12.697	0.038	12.680	0.050
116.51448	-38.01421	13.498	0.009	13.419	0.013	13.381	0.045	13.579	0.080
116.54938	-38.21002	11.339	0.005	11.312	0.005	11.275	0.014	11.218	0.016	11.221	0.127
116.56459	-37.74740	12.325	0.006	12.312	0.007	12.339	0.028	12.239	0.037
116.57994	-37.56290	11.977	0.006	11.911	0.031
116.58564	-37.96366	13.892	0.013	13.785	0.019	13.788	0.088	13.711	0.122
116.60560	-38.23373	14.052	0.013	13.853	0.016	13.681	0.076	13.519	0.083
116.61145	-38.10934	12.265	0.005	12.198	0.007	12.130	0.025	12.139	0.037
116.66325	-38.32594	13.385	0.009	13.300	0.058
116.66850	-38.04359	12.217	0.006	12.233	0.008	12.193	0.027	12.147	0.050
116.67281	-37.84615	12.832	0.007	12.574	0.008	12.434	0.029	12.514	0.043
116.67488	-37.98390 (#13)	12.227	0.005	12.230	0.007	12.081	0.021	12.105	0.041	10.955	0.072
116.68185	-38.28975	11.682	0.004	11.726	0.018
116.68972	-37.82607	11.071	0.004	11.073	0.004	11.063	0.011	11.020	0.014
116.69822	-38.00890	13.726	0.011	13.540	0.014	13.406	0.057	13.888	0.158
116.72084	-37.71950	11.653	0.004	11.633	0.006	11.616	0.019	11.574	0.022
116.72728	-37.59192	11.864	0.006	11.802	0.025
116.73331	-38.35595	9.071	0.003	9.068	0.039
116.74249	-37.63916 (#18)	10.586	0.003	10.587	0.004	10.589	0.009	10.578	0.010	10.302	0.059
116.75339	-37.96264	13.379	0.010	13.279	0.012	13.266	0.053	13.330	0.081
116.76585	-37.96487	12.370	0.006	12.367	0.008	12.292	0.027	12.268	0.043
116.77636	-37.73380	12.111	0.006	12.096	0.008	12.045	0.023	12.120	0.040
116.79779	-37.79682
116.81857	-38.30363	10.169	0.002	10.152	0.007
116.84155	-38.30055	12.075	0.005	12.043	0.022
116.84765	-37.71917
116.86294	-38.13213
116.92513	-38.18621
116.94233	-38.15534

TABLE 6 — *Continued*

RA J2000	DEC J2000	[3.6] mag	σ ([3.6]) mag	[4.5] mag	σ ([4.5]) mag	[5.8] mag	σ ([5.8]) mag	[8.0] mag	σ ([8.0]) mag	[24] mag	σ ([24]) mag
116.94269	-37.51560
116.94462	-37.88126
Members from Hünsch et al. (2003)											
115.95710	-37.96688	9.491	0.002	9.460	0.003	9.460	0.005	9.456	0.006	9.345	0.036
116.03583	-37.98349	9.044	0.003	9.059	0.003	9.044	0.004	9.011	0.004	9.073	0.032
116.07976	-38.00541	11.294	0.004	11.269	0.005	11.215	0.013	11.226	0.018
116.15953	-38.22106	9.010	0.002	8.985	0.003	8.932	0.004	8.922	0.004	8.839	0.033
116.20300	-38.09869	11.365	0.004	11.459	0.005	11.417	0.015	11.325	0.018
116.21267	-37.66869 (#15)	9.797	0.003	9.883	0.007	9.755	0.005	9.285	0.034
116.36051	-38.19643 (#19)	10.036	0.003	10.056	0.003	10.017	0.007	10.029	0.007	9.704	0.038
116.38235	-37.50727	10.648	0.069
116.39170	-37.79194	11.008	0.004	11.017	0.004	10.964	0.011	10.953	0.014	10.912	0.069
116.50776	-38.00752 (#16)	10.562	0.004	10.540	0.004	10.495	0.009	10.474	0.010	9.983	0.043

numbers next to the coordinates designate 24 μ m excess sources from Table 7